ANNUAL REVIEWS

Annual Review of Chemical and Biomolecular Engineering

Drying Drops of Colloidal Dispersions

Sumesh P. Thampi and Madivala G. Basavaraj

Department of Chemical Engineering and Center for Soft and Biological Matter, Indian Institute of Technology Madras, Chennai, India; email: sumesh@iitm.ac.in, basa@iitm.ac.in

Annu. Rev. Chem. Biomol. Eng. 2023. 14:53–83

First published as a Review in Advance on March 14, 2023

The *Annual Review of Chemical and Biomolecular Engineering* is online at chembioeng.annualreviews.org

https://doi.org/10.1146/annurev-chembioeng-101121-085056

Keywords

sessile drop evaporation, evaporative patterns, evaporation-driven flows, drying of complex fluids, drying in complex configurations

Abstract

Drying drops of colloidal dispersions have attracted attention from researchers since the nineteenth century. The multiscale nature of the problem involving physics at different scales, namely colloidal and interfacial phenomena as well as heat, mass, and momentum transport processes, combined with the seemingly simple yet nontrivial shape of the drops makes drying drop problems rich and interesting. The scope of such studies widens as the physical and chemical nature of dispersed entities in the drop vary and as evaporation occurs in more complex configurations. This review summarizes past and contemporary developments in the field, emphasizing the physicochemical and hydrodynamical principles that govern the processes occurring within a drying drop and the resulting variety of patterns generated on the substrate.

1. INTRODUCTION

Evaporating liquid drops are ubiquitous. Raindrops (water drops falling through air), fog (tiny water drops suspended in air), and dew (water drops condensed on the surface of grass, spiderwebs, etc.) are common examples of natural phenomena involving drops. The fate and transport of drops generated during natural human activities such as breathing, coughing, sneezing, and talking are of interest in the context of airborne diseases such as coronavirus disease 2019 (COVID-19), measles, or tuberculosis. Chemical and other engineering processes that involve drops comprise various types of spray operations, such as drying, coating, painting, atomization, two-phase flows in columns, and droplet microfluidics. Typically, drops generated during natural or human-made processes encountered in day-to-day life are (*a*) suspended in a stagnant or moving fluid, (*b*) flowing through a narrow channel, or (*c*) residing on surfaces. Drops suspended in a stationary fluid may assume a spherical shape, depending on their Bond number. The Bond number is the ratio of gravitational force to surface tension force and is given by $R_d^2 \Delta\rho g/\sigma$, where R_d is the characteristic size of the drop, $\Delta\rho$ is the density difference between the liquid and the surrounding fluid, g is acceleration due to gravity, and σ is the interfacial tension between the drop and the surrounding fluid. Similarly, a drop placed on a rigid solid substrate assumes a spherical cap shape when the liquid that constitutes the drop partially wets the solid substrate and the Bond number is smaller than one.

Liquid drops generated in unit operations and processes relevant to chemical process industries, food technology, medicine, biology, and other disciplines usually contain dissolved or dispersed components or a combination of both. This is also the case for respiratory drops. The nature of the dissolved or dispersed species is specific to the intended use of the drops in a particular process. Evaporating liquid drops containing nanoparticles or colloids, polymers, surfactants, proteins, DNA, blood cells, bacteria, viruses, salt and other soluble matter, and so forth have been the subject of considerable scientific exploration via experiments, theory, and simulations for more than two decades. Most recently, investigators have studied the lifetime and evaporation of virus-loaded drops generated by humans and animals in the context of understanding the spread of COVID-19. The transport of pathogen-loaded drops through air as an aerosol or deposited on solid surfaces is a complex problem that requires the attention of researchers across engineering and scientific disciplines. When the liquid from drops containing dissolved or dispersed material evaporates, a residue of these materials is left behind. When drops dry on solid substrates, the spatial distribution of the solids in the final deposit is typically referred to as an evaporative pattern or evaporative stain. The study of evaporation-driven pattern formation when drops are dried has generated considerable interest because of its relevance in diverse areas including, but not limited to, disease diagnostics, forensics, adulteration detection, surface patterning, fabrication of colloidal crystals, electrochemical sensing and electrocatalysis, paint formulation, and printing technology. To date, most of these studies have focused on achieving control over the distribution of solids in evaporative deposits.

The spatial distribution of solids in dried deposits that are dispersed uniformly or present as molecular species in the drops prior to complete evaporation of the solvent is dictated by the transport processes (i.e., momentum, heat, and mass transport) that occur in the drying drops. Some of the most common transport processes that arise when drops dry on solid substrates are evaporation-driven flow of solvent due to pinning of drops to the solid surface, fluid flows driven by a gradient in surface tension, loss of mass of the solvent via evaporation, evaporative cooling and associated thermal Marangoni flows, and mass transfer due to condensation when drops dry in a high-humidity environment. Dispersed species such as particles in a drying drop respond to these processes, leading to particle transport. In addition, dissolved species in a drop can precipitate

out of the solution as its concentration increases, leading to crystallization. Therefore, although evaporation of liquid drops on solid surfaces may appear simple, it encompasses many coupled processes central to chemical engineering.

The remainder of this review is organized as follows. In Section 2 we provide a historical perspective of the drying drop problem. Next, in Section 3, we present an analysis of the variety of patterns formed when a sessile drop of colloidal dispersion in contact with a substrate is dried. We then discuss the heat and momentum transport processes in spherical and sessile drops and describe the origin of the convective and Marangoni flows in Sections 4 and 5. In Section 6, we describe recent developments in the study of various complex fluids subjected to drying processes, and in Section 7, we discuss the study of drying processes in complex configurations. We conclude in Section 8 with a brief summary of our current understanding of the field and the scope for future development. This review is certainly not exhaustive and cannot accommodate all developments in the field. Therefore, we refer the reader to excellent reviews that have appeared in the literature from time to time (for reviews from the past decade, see 1–13).

2. HISTORICAL OVERVIEW

The first reference to the motion of particles in an evaporating liquid drop containing dispersed particles appears in a report by Robert Brown published in 1829 (14). This report names the evaporation of liquid as the principal cause of particle motion. Brown argues that the fluid current that is responsible for particle transport is directed from the center to the circumference. Particle motion in the initial stages of evaporation is reported to be minimal or imperceptible, becoming more obvious at later stages. Toward the final stages of evaporation, the convective currents are observed to be very rapid. Such intriguing particle motion occurs in particle-laden drops exposed to air, but not when such drops are immersed in oil, a conclusive proof of the existence of evaporation-driven flows. These phenomenal experimental observations on drying particle-laden drops, although qualitative in nature, clearly demonstrate (*a*) the motion of particles from the center toward the circumference or the edge and (*b*) a substantial increase in particle velocity in the final stage of evaporation.

In 1956, Vanderhoff & Gurnee (17) used an optical microscope to examine the evaporation of aqueous dispersion drops (1% concentration) containing monodisperse latex particles with a diameter of 1.2 μm. As solvent evaporated from the drop, the latex particles were found to arrange at the edge of the drop in a close-packed manner. The deposition process was spontaneous, with the particles forming regular hexagonal arrays. Kulnis & Unertl (15) reported experiments demonstrating the arrangement of particles in the dried deposit formed by the evaporation of sessile drops containing 0.1% polystyrene particles by volume on a freshly cleaved mica surface. **Figure 1*a***, imaged by a surface force microscope, shows a close-packed band of polystyrene particles, with a thickness of a single particle, intersecting with another band of particles. These authors do not discuss the distribution of particles across the area of the deposit, nor do they mention the location of the particle bands shown in **Figure 1*a***.

In 1994, El Bediwi et al. (16) reported an atomic force microscopy investigation of particle-laden drops dried on solid substrates of different wettabilities. These authors studied the drying of aqueous dispersions of model colloidal spheres (styrene-butadiene latex, 160–190 nm in diameter) on glass, mica, calcite, and cellophane substrates. **Figure 1*b*** depicts an arrangement of particles in the deposit formed by drying 0.5 μL drop (9.6×10^{-6} volume fraction) on a cellophane surface. A band of densely packed particles is visible at the edge of the drop. El Bediwi et al. hypothesized that as water evaporates from the drop, an outward flow directed toward the edge is set up. The inhomogeneous distribution of particles in the dried deposit (i.e., the presence of more particles at

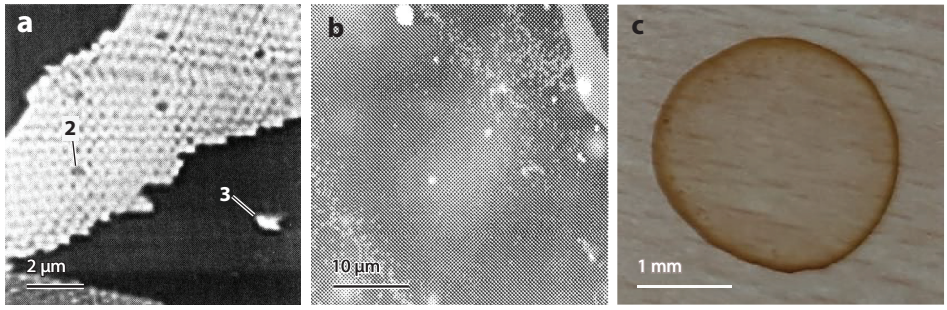

Figure 1

(*a*) A surface force microscopy image of an 10 μm × 10 μm area showing an arrangement of polystyrene (PS) particles at the edge of the deposit, formed by drying dispersion of PS particles on a mica surface at 20°C (15). The monolayer deposit is labeled 2. (*b*) An atomic force microscopy image of the dried deposit, consisting of styrene-butadiene latex with a diameter of 160–190 nm, formed on a cellophane surface. A band of particles at the edge of the deposit is visible at the top right corner (16). (*c*) A typical dried pattern resulting from the evaporation of volatile liquid from a spilled drop of coffee.

the edge compared with the interior of the deposit) is attributed in part to the change in fluid–air surface tension and capillary forces during evaporation.

Deegan et al. (18, 19) provided the first comprehensive analysis of the drying of particle-laden drops on solid substrates. **Figure 1*c*** shows the deposit that forms when liquid from a coffee drop spilled on a solid surface, such as a table or a saucer, is completely lost due to evaporation. The results show that the accumulation of particles at the edge of the dried pattern is not limited to drops containing colloidal-scale particles. The formation of a distinct ring-shaped deposit is evident even though the coffee particles in the drops are initially distributed uniformly. Deegan et al. discuss the connection between the drying of drops containing colloids and coffee spills, which led to the introduction of terms such as the coffee-stain effect and coffee-ring formation.

These studies also put forward the conditions under which edge or peripheral deposits typically form. First, the continuous medium in which the particles are dispersed must evaporate. Second, when placed on a solid substrate, the drop should have a nonzero contact angle. Third, the contact line of the drop must be pinned to the initial position during the course of drying. During the evaporation of solvent from drying drops, the contact line on the substrate may move; however, this movement may not always be smooth. Since no substrates are atomically smooth, their surfaces will always possess physical and chemical heterogeneities. Such heterogeneities can inhibit the local motion of the contact line, resulting in pinning of the contact line on the substrate. Depending on the strength of pinning, two different modes of evaporation may be observed. The first is the constant contact radius (CCR) mode, in which the contact line remains pinned during the observation window. Correspondingly, the contact angle systematically decreases (**Figure 2*a***). The second is the constant contact angle (CCA) mode, in which the contact line is not pinned. Instead, the contact line continuously recedes, and the contact angle remains constant throughout the observation window (**Figure 2*b***). Surface tension forces maintain the equilibrium contact angle, θ, during this process. In general, most of the experiments show that particle-laden drops evaporate via a combination of CCA and CCR modes. The drying of drops in CCR mode is a prerequisite for the formation of ring-shaped deposits. The outward flow of solvent (see Section 4) that carries the particles from the drop interior to the edge, as imaged by time-resolved microscopy, conclusively proves that ring deposits form as a consequence of the flows generated due to loss of liquid from drops evaporating on solid substrates. In addition, the mass of particles

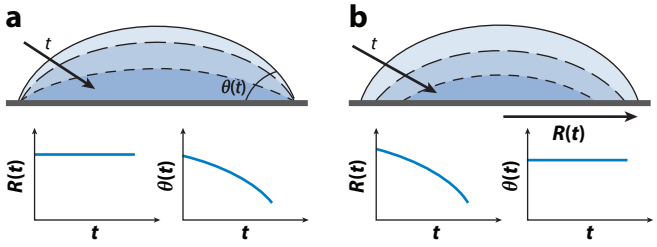

Figure 2

Schematic representation of a side view of drops evaporating in (*a*) constant contact radius mode and (*b*) constant contact angle mode. The solid line represents the initial drop shape profile (at $t = 0$), and the dashed lines represent the drop shape profiles as drying proceeds. The evolution of the contact radius, $R(t)$, and of the contact angle, $\theta(t)$, during the course of evaporation in each mode are shown on the bottom.

in the ring increases with time in a power-law fashion, regardless of the type of particle, dispersion medium, or substrate wettability.

Although detailed (albeit qualitative) accounts of particle motion in drying drops date back to 1829, insights into the physics of hydrodynamic flows in evaporating drops, the exponential increase in research in this area, and the application of drying-induced pattern formation in various disciplines are certainly due to the remarkable contributions of Deegan et al. (18, 19).

3. EVAPORATION OF PARTICLE-LADEN DROPS: TYPICAL DRYING PATTERNS

Research over the past 25 years has established that the particle distribution in deposit patterns left by drops dried on a solid, nonporous substrate is determined by numerous parameters. These include (*a*) the drop configuration, such as drops residing on a horizontal substrate (sessile drops), inverted or hanging drops (pendant drops), or drops on inclined surfaces; (*b*) particle concentration, size, and shape; (*c*) the properties of the carrier fluid; (*d*) environmental conditions such as temperature and humidity; (*e*) the temperature of the substrate and properties such as wettability and surface roughness; (*f*) the presence of salt, surfactant, or other species along with the particles; and (*g*) external fields (e.g., electric, magnetic, gravitational, or acoustic). We refer the reader elsewhere for more details on these aspects (4, 8, 20–27).

A plethora of evaporation-driven deposit patterns have been reported. Here, we summarize some commonly observed characteristic deposit patterns that form when particle-laden drops are dried. **Figure 3** presents two-dimensional (2D) low-magnification microscopy images of different types of dried deposits, along with one-dimensional (1D) height profiles. The distribution of particles in the patterns can be quantified in terms of number density, defined as the number of particles per unit area. 1D intensity profiles have also been used as a qualitative indicator of particle distribution in dried deposits. **Figure 3*a–e*** depicts the drying of a dilute aqueous dispersion of hematite ellipsoids. The dried deposits' visually appealing color is due to the inherent reddish color of the iron oxide particles, providing qualitative evidence of the distribution of dark red and pale yellow colors representing, respectively, higher and lower concentrations of particles in the pattern.

Figure 3*a* shows the coffee-ring or coffee-stain pattern, most commonly seen when drops dry in a sessile configuration. In these deposits, most of the particles are present at the edge or periphery (which appears as hills in the height profile), with very few or no particles in the interior region of the deposit (flat region in the height profile). If the particles in the drying drop are too large (~10-μm-diameter polystyrene particles with a density of 1,050 kg/m^3), then sedimentation interferes with the particle transport to the edge (30). In addition, colloidal (particle–particle

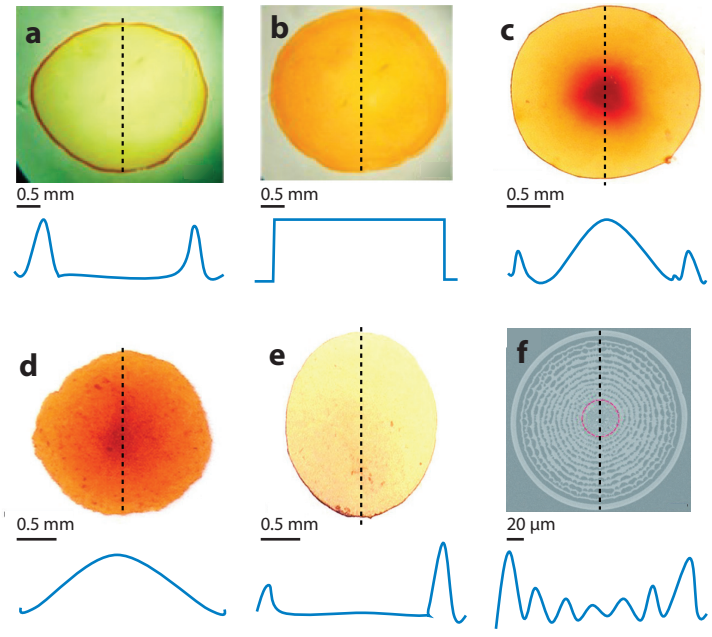

Figure 3

Two-dimensional (2D) low-magnification micrographs showcasing different types of dried deposit patterns formed by drying of particle-laden drops on nonporous solid surfaces. (*a*) Coffee rings or coffee stains. (*b*) Uniform deposits. (*c*) Coffee-eye deposits. (*d*) Central dome. (*e*) Asymmetric deposits. (*f*) Multiple rings. One-dimensional (1D) representative height profiles that provide evidence of typical distribution of particles in the deposit are shown as continuous solid lines below each pattern. Each 1D profile illustrates the height distribution along the dashed vertical line in each pattern. Panels *a* and *b* adapted with permission from Reference 31. Panels *c*–*e* adapted with permission from Reference 28. Panel *f* adapted with permission from Reference 29.

and particle–substrate) interactions dictate the formation of coffee-ring deposits. When both particle–particle and particle–substrate interactions are repulsive, there is neither particle–particle aggregation nor adhesion of particles to the solid substrate; as a result, coffee-ring formation is favored (25, 31). A recent study showed that the drying of drops containing microgel particles at highly dilute concentrations leaves monolayer or single-particle-thick coffee rings (32). Such monolayer coffee-ring deposit patterns form when (*a*) the particles in the drying drops are surface active, such that they spontaneously adsorb to the drop surface, and (*b*) the concentration of particles in the drop is below the monolayer concentration, which is the particle concentration sufficient to cover the entire area of the drop surface. Monolayer coffee rings can also form when highly dilute dispersions of nondeformable particles are dried (30).

Further investigations into the structure of coffee-ring deposits have revealed various particle arrangements. As discussed in Section 4.4, below, the deposition is driven primarily by convective flows to the pinned contact line. If the timescale of convection is much shorter than the Brownian timescale of the particles, then a disordered arrangement of particles is obtained. On the other hand, a crystalline arrangement is obtained if the convective flows are slower. A significant fraction of particles are incorporated into the coffee ring during "rush hour," wherein the flow velocities are relatively large and, hence, the resulting particle arrangement during this period is amorphous (33). Therefore, reducing the duration of the rush hour (say, by using a less wetting surface) as well as increasing the diffusion process of dispersed particles can help in the crystallization of particles

in the coffee ring. The crystalline arrangement itself may vary (say, from square to hexagonal particle packing; 33) in a given ordered deposit. However, general guidelines, or even the possibility of the existence of such guidelines, for obtaining a crystalline arrangement of particles in other kinds of deposits are not known. The order–disorder transition in the arrangement of particles has also been observed in deposits of colloidal rods and soft-microgel particles (32, 34).

The suppression of coffee-ring formation can lead to uniform deposits (**Figure 3*b***). In these patterns, particles are homogeneously distributed throughout the deposit area. In other words, the number density of particles in such deposit patterns, on average, is the same everywhere. The coffee-ring formation can be suppressed by inducing particle motion away from the contact line. Such motion can be generated by several methods, including substrate heating, subjecting drops on the substrate to surface acoustic waves or oscillations, and adding surfactant or surface-active polymers. Therefore, the relative strengths of (*a*) the flow that drives the particles away from the contact line and (*b*) the outward radial flow that depends on the contact angle of the droplet and drives the particles toward the contact line dictate the distribution of particles in the dried deposit.

One of the most relevant applications of studies of pattern formation via drying drops involves suppressing the coffee ring and obtaining a uniform deposit of particles. Several factors are known to inhibit coffee-ring formation: Marangoni flows (35), nonspherical particles (36), addition of surfactants (24, 37), addition of polymers (polymer brush) (38, 39), heating of the substrate (40–42), continuous depinning by the addition of salt (43) or sugar (44), use of nonwetting surfaces (45), interfacial adsorption of particles (32), and modulation of the surface charge of the particles and substrate (25, 31). The formation of a viscoelastic network of particles on the drying drop surface influences the flow field in the drop and facilitates suppression of coffee-ring formation (36, 46). The inward Marangoni flow that inhibits the accumulation of particles at the contact line can also arise when the drying drops contain surface-active molecules such as surfactants (24, 34, 37, 47). The microstructure of the deposits shows coffee-ring and uniform deposits when dispersion drops containing similarly and oppositely charged particle–surfactant mixtures, respectively, are dried (48). In the latter case, the nature of the pattern depends on the concentration of the surfactant, the interplay between Coulombic and hydrophobic interactions, and the adsorption of particles to the interface.

In the coffee-eye deposits shown in **Figure 3*c***, along with the formation of a thin coffee stain at the edge, there is an accumulation of particles in the central region. The central stain is typically thicker than the outer ring. The evaporation of particle-laden drops on heated substrates (49) and deposits formed by drying drops in pendant configuration (28) leave such deposit patterns.

The temperature of the environment in which drops are dried and the temperature of the substrate can significantly influence the distribution of particles in deposit patterns. Aqueous drops containing 216-nm-diameter polystyrene particles evaporated on a silicon wafer (contact angle, $\theta = 43°$) at controlled humidity (50% relative humidity) have been observed to leave coffee-ring patterns with more than 90% of the particles deposited at the edge when the temperature of the drying environment is $T = 25°C$. In contrast, a uniform deposit forms when $T = 75°C$ (49). The formation of uniform deposits has been argued (42) to be due to interfacial capture of the particles by the water–vapor interface, which descends rapidly when the drops are dried in a high-temperature environment. The evaporation of water drops with ~100-nm-diameter spherical polystyrene particles, when dried on a substrate maintained at 30°C, forms typical coffee stains. However, coffee-eye patterns form when evaporation occurs on a heated substrate ($T = 80°C$), with all other parameters being identical (49). These coffee-eye patterns form as a result of the inward Marangoni flow that is created when drops evaporate on substrates with a temperature higher than that of the surrounding environment. In such cases, the temperature of the drop at the contact line will be highest and the surface temperature will decrease along the vapor–liquid

interface, lowest at the drop apex (49, 50). This temperature gradient leads to a surface tension gradient that then induces flow from the contact line toward the center of the drop (see Section 4.4), causing particles to accumulate in the center of the deposit. Therefore, the patterns obtained from drying drop experiments at elevated temperatures also depend on the interplay between the thermal Marangoni flow (49, 50) and the interfacial adsorption of particles due to higher evaporation rates (42).

Particle distribution in dried deposits can be controlled by subjecting the evaporating drops to external forces such as surface acoustic waves (51). While coffee-ring patterns tend to form when dispersion drops dry in the absence of external stimuli, particle-laden drops drying in the presence of surface acoustic waves with a frequency of 9.7 MHz leave a central dome–like deposit. In stark contrast, the application of 20-MHz surface acoustic waves to evaporating dispersion drops results in a uniform or disclike deposit pattern. The force generated due to the surface acoustic field drives the particles in the drying drops toward the nodes of the standing waves and oppose particle transport due to outward radial flows that drive the particles to the edge. Therefore, the morphology of the evaporative patterns and the suppression of coffee rings depend on the strength of the surface acoustic field (51).

Drying of particle-laden drops on high-contact-angle substrates leaves a deposit with a mountain-like appearance, typically referred to as a central dome deposit (28) (**Figure 3*d***). In central dome deposits, the concentration or number density of particles at the center is highest and the concentration of particles decreases monotonically from the center to the edge. Typically, in such deposits there are very few or no particles at the contact line. When drying drops contain considerably large or dense particles, they sediment under gravity. In this case, the mountain naturally forms because the number of particles settling near the center of the deposit is larger than elsewhere. Mountain-like deposits can also form as a result of continuous depinning of the contact line (52).

On average, the deposit patterns shown in **Figure 3*a–d*** are azimuthally symmetric. In other words, the height profile would look similar if the vertical lines at any other orientation or angle were considered. Asymmetric deposit patterns form when drops dry on inclined substrates (28, 53–55); **Figure 3*e*** presents an example. In Section 7, we briefly discuss the origin of such deposits with higher concentrations of particles on one side of the pattern.

Dried deposit patterns can have multiple rings (29) (**Figure 3*f***). Different mechanisms underlying the formation of concentric rings have been postulated. When a drop of pure fluid evaporates, the contact line remains pinned to the substrate. If the drop contains dispersed particles, a deposit forms; thereafter, the contact line is no longer pinned directly to the substrate but rather on the edge of the solid deposit itself. The free-hanging surface near the contact line can then change its shape from convex to concave as evaporation proceeds. This dimple in the interface shape can drive converging flows, bringing the particles toward the dimple. The interface can also rupture at the location of the dimple. That would mean that the pinning location has changed from the initial pinning point to a new location. This process of pinning, depinning, and repinning can occur repeatedly, leading to several concentric rings in the deposit (29, 56–58).

This mechanism has been demonstrated in solutions of DNA (59), but it is not clear whether repeated instances of pinning occur in other scenarios that have reported formation of concentric rings. Moreover, the factors that determine the location of the dimple and whether dimple formation is the cause of depinning have not been addressed either theoretically or numerically.

Concentric rings of deposits may also form as a consequence of changes in the rheological properties of the colloidal dispersion being dried. As the drop evaporates, the concentration of particles inside the drop increases. Correspondingly, the viscosity of the dispersion also dramatically increases (diverges). At high particle loading, as evaporation proceeds, the increased

viscosity of the dispersion can slow down convection currents and prevent the deposition of particles at the contact line. Periodic arrays of deposits have been predicted theoretically (60), but this mechanism lacks experimental support. While the above discussion describes the possible mechanisms of concentric-ring formation in the final deposits, evaporation in confined geometries can also lead to concentric and connected rings (spirals). In such cases, the patterns seem to emerge from the modified pinning or depinning behavior of the confining surfaces (57, 61).

In this section, we have highlighted several recent contributions to research on evaporation-driven deposition of colloidal particles. The literature in this area is extensive, and we refer readers to several dedicated reviews for more details (4, 8, 20–24, 62).

4. TRANSPORT PROCESSES IN EVAPORATING DROPS

The previous section discusses the variety of patterns formed by drying drops of colloidal dispersions. The primary driving force for the whole process is evaporation of the solvent. In this section, we describe how flows arise as a result of solvent evaporation that can advect and deposit entities dispersed in the drop to generate different patterns.

4.1. Spherical Drops

We start by analyzing the case of a spherical drop. When a drop of liquid suspended in unsaturated air evaporates, the liquid molecules escape into the surrounding air. Typically, the drop remains spherical throughout the evaporation process because of its large surface tension. As a consequence, evaporation is isotropic and the drop acts as a source of mass to the surrounding medium. The rate of evaporation is dictated by the difference in chemical potential of the molecules between the drop and the vapor medium. Clearly, the evaporation kinetics and, thus, the lifetime of the drop (i.e., the time required for the drop to completely vaporize) are influenced by several factors: (*a*) molecular diffusivity and vapor concentration in the surrounding medium, (*b*) temperature and heat transport in the drop and in the surrounding medium, and (*c*) the thermodynamic and transport properties of the drop–air interface.

The diffusion of molecules from the drop surface to the surrounding vapor phase can be analyzed as follows. As shown in **Figure 4*a***, concentric spherical surfaces to the drop represent surfaces of constant concentration, while radial lines orthogonal to these isosurfaces, referred to as flux lines, indicate the direction of the diffusive flux of the vapor molecules. No mass transfer

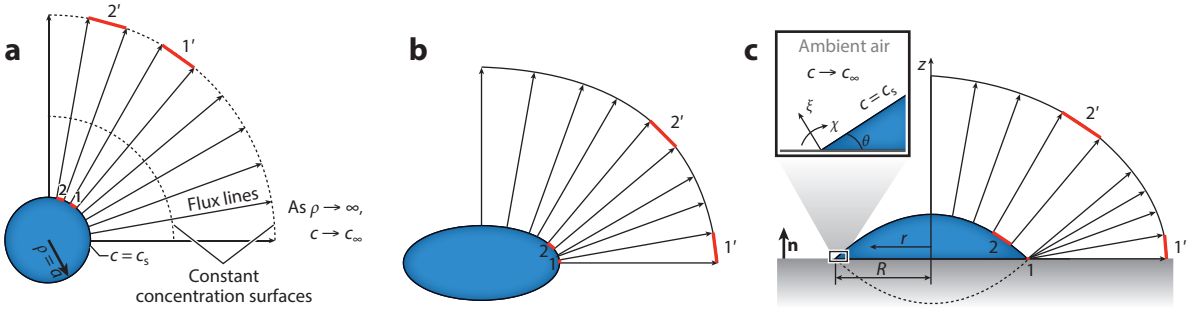

Figure 4

Schematics illustrating the diffusion of vapor to the surrounding, quiescent air from (*a*) an evaporating free-standing spherical drop, (*b*) an evaporating free-standing ellipsoidal drop, and (*c*) an evaporating sessile drop deposited on a substrate. The flux lines emanate from the surface of the drop. There is no mass transfer across the flux lines. In each case, the evaporated mass from sections 1 and 2 escapes through sections 1′ and 2′, respectively, but with a reduced flux because the latter sections have larger surface areas than the former.

takes place across the flux lines; therefore, the mass flow rate between the flux lines must be conserved. In other words, the mass flow rate through the sections labeled 1 and 1′ in **Figure 4*a*** must be the same. This is possible only if the diffusive flux decays as ρ^{-2}, since the area of a spherical surface increases as ρ^2, where ρ is the radial distance measured from the center of the drop. This is equivalent to stating that concentration of vapor molecules $c(\rho)$ decays as ρ^{-1}, since the diffusive flux is proportional to the gradient of concentration, according to Fick's first law. In other words, we can write the vapor concentration profile around an evaporating drop as $c(\rho) - c_\infty = (c_s - c_\infty)(a/\rho)$, which satisfies both the governing equation $\nabla^2 c = 0$, where ∇^2 is the Laplacian operator, and the boundary conditions (*i*) on the drop surface, $\rho = a$ and $c = c_s$, and (*ii*) as $\rho \to \infty$, $c = c_\infty$. Note that these arguments rely on the facts that (*a*) the surface of the drop is saturated with vapor molecules, where the corresponding concentration is c_s, and (*b*) the vapor diffusion is a quasi-steady process in which convection around the drop plays no role.

The evaporative flux corresponding to this algebraically decaying concentration profile is $J(\rho) = -D_v \mathrm{d}c/\mathrm{d}\rho$, where D_v is the diffusivity of the vapor molecules in the surrounding medium. Specifically, the flux on the drop surface (at $\rho = a$) can be determined as $D_v(c_s - c_\infty)/a$. Thus, the evaporative flux is inversely proportional to the radius of the drop—the smaller the drop, the larger the evaporative flux! On the other hand, in accordance with Langmuir's calculation (63), the total rate of evaporation from the drop is proportional to a because it is determined as the product of the flux at the surface ($\propto a^{-1}$) and the surface area ($\propto a^2$). Thus, larger drops evaporate faster, but the evaporation rate is proportional only to the size of the drop and not to its surface area.

4.2. Sessile Drops

Consider again the vapor concentration profile around an evaporating spherical drop. As shown in **Figure 4*a***, the mass flow rate through sections 1′ and 2′, which span the same differential solid angle, will be the same. Moreover, the mass flow rate through section 1 (or 2) must be the same as that through section 1′ (or 2′) because there is no mass transfer across flux lines. This situation can be contrasted to that of flux lines from a nonspherical drop. For a spheroidal drop (**Figure 4*b***), equal mass flow rates through sections 1′ and 2′ demand greater mass flux through section 1 versus 2 because section 1 is smaller than section 2. This difference in the mass flux through sections 1 and 2 is a manifestation of the fact that the vapor flux from a curved surface is directly dependent on the local curvature of the surface (10). Thus, regions of greater curvature, such as section 1, will generate a larger evaporative flux in comparison to regions of lesser curvature, such as section 2. This effect is even more pronounced for a sessile drop and can be understood as follows. Evaporation from a sessile drop is mathematically equivalent to evaporation from a freely suspended liquid lens (no substrate) (**Figure 4*c***). This equivalence arises because zero vapor flux normal to the rigid substrate ($\mathbf{J} \cdot \mathbf{n} = 0$) on which the sessile drop resides translates into a symmetry boundary condition ($\nabla c \cdot \mathbf{n} = 0$) of the liquid lens. Here, $\mathbf{n}$ is defined as unit normal to the substrate. Then, as shown in **Figure 4*c***, the curvature is infinite at the tip of the liquid lens (i.e., at the contact line of the sessile drop), leading to a singularly large vapor flux through the point cross section 1. In other words, the evaporative flux from the surface of a sessile drop is not uniform; it is lowest at the apex and highest near the contact line.

The inhomogeneous evaporative flux from the surface of the sessile drop forms a cornerstone of our present understanding of coffee-ring formation (18, 19). To proceed analytically, we focus on a region close to the contact line (**Figure 4*c***), and we define a local polar coordinate system (ξ, χ). By neglecting the curvature of the contact line and the interface, we can assume the geometry of the drop near the three-phase contact line to be a wedge. Under quasi-steady conditions, the vapor concentration is governed by $\nabla^2 c(\xi) = 0$ with the following boundary conditions: (*i*) $\mathbf{n} \cdot \nabla c(\xi, \chi = 0) = 0$, (*ii*) $c(\xi, \chi = \pi - \theta) = c_s$, and (*iii*) $c(\xi \to \infty, \chi) = c_\infty$. Using the standard

separation of variables method for linear partial differential equations and applying the boundary conditions, we obtain the vapor concentration profile around the contact line region as follows:

$$c(\xi, \chi) = c_s + \sum_{k=0}^{\infty} a_k \xi^{\frac{(2k+1)\pi}{2(\pi-\theta)}} \cos\left(\frac{(2k+1)\pi}{2\theta}\chi\right), \quad 1.$$

where a_k are coefficients to be determined from the far-field boundary conditions. Since the calculations are focused near the contact line, Equation 1 is valid for low values of ξ, and $k = 0$ will be the dominant term in the series. As for the case of spherical drops, the evaporative flux on the surface of the drop can now be calculated as $J(\xi) \propto \xi^{[(2k-1)\pi+2\theta]/(2\pi-2\theta)}$. Interestingly, for $k = 0$, $J(\xi)$ diverges at $\xi = 0$ for $\theta < \pi/2$. While $\xi = 0$ is a theoretical limit, in reality the contact line is of some finite thickness (say, δ) and may provide a cutoff length scale to the mathematical divergence. Thus, the maximum evaporative flux from the contact line would be $J(\xi) \propto 1/\sqrt{\delta}$ when $\theta \approx 0$.

A sessile drop that is not deformed by gravity or viscous stresses due to fluid flows (the Bond number and capillary number are much less than one) adopts the shape of a spherical cap. In this case, under the quasi-steady approximation, the vapor flux (64) as a function of radial coordinate r (**Figure 4*c***) can be exactly calculated using the separation of variables method in toroidal coordinates:

$$J(r) = J_0\left[\frac{\sin\theta}{2} + \sqrt{2}(\cosh\alpha + \cos\theta)^{\frac{3}{2}} \int_0^{\infty} \frac{\cosh\theta\tau \tanh\beta\tau}{\cosh\pi\tau} P_{-\frac{1}{2}+i\tau}(\cosh\alpha)\tau \mathrm{d}\tau\right], \quad 2.$$

where $J_0 = D_v(c_s - c_\infty)/R$, $\beta = \pi - \theta$, $P_{(-1/2)+i\tau}(\cosh\alpha)$ is the Legendre function of the first kind, and α is a toroidal coordinate given as $r = R\sinh\alpha/[\cosh\alpha + \cos\theta]$. For small contact angles, Equation 2 reduces to $J(r) = (2/\pi)J_0/\sqrt{1-(r/R)^2}$, illustrating the diverging nature of the vapor flux near the contact line ($r \to R$). As a replacement for Equation 2, $J^a(r) = J_0[0.27\theta^2 + 1.30][0.6381 - 0.2239(\theta - \pi/4)^2][1 - r^2/R^2]^{(\theta/\pi)-(1/2)}$ has been suggested (65) as a partially empirical fit for $J(r)$ that produces <6% error.

The enhancement in the evaporative flux due to curvature effects becomes even more apparent if deformed sessile drops are considered. Such drops can be prepared by having the drops sit on noncircular pedestals (66). Both numerical and experimental investigations (66) have shown that not only the volume or surface area but also the shape of the sessile drop itself (particularly the presence of curved regions) has to be taken into account to explain the observed evaporation rates.

4.3. Evaporation-Driven Heat Transfer in Sessile Drops

The latent heat of vaporization of the liquid, H_v, must be drawn from the sensible heat available in the drop, the substrate, and the surrounding vapor. Since the evaporative flux from the drop surface is nonuniform, the heat requirement to sustain the evaporation is also uneven, leading to temperature variations on the surface of the drop. In addition, the path length for conductive heat transfer from the substrate to the drop surface is not constant—the path is longest at the apex and shortest at the contact line. For these two reasons, temperature profiles inside the drop are time dependent and the profiles may change qualitatively as the drop evaporates.

Considering the sessile drop and the substrate as a composite medium for heat transfer, one can calculate the temperature profile at the surface of a thin drop (for small θ) as (35)

$$T - T_\infty = H_v J^a(r,\theta)\left(\frac{h(r)}{k_l} + \frac{h_s}{k_s}\right)\sqrt{1 + \left(\frac{\partial h}{\partial r}\right)^2}, \quad 3.$$

where T_∞ is the ambient temperature; $h(r)$ and h_s are the drop surface profile and the substrate thickness, respectively; and k_l and k_s are the thermal conductivities of the liquid and substrate,

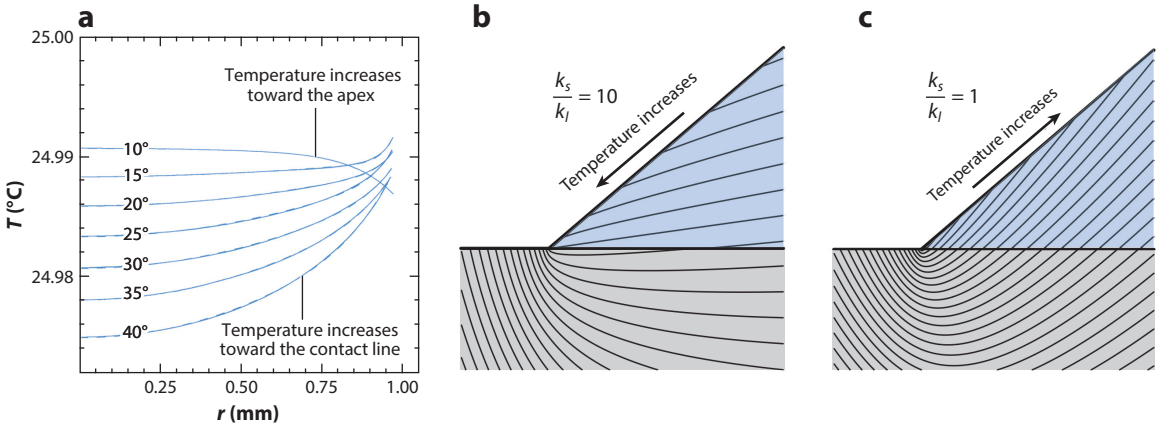

Figure 5

(*a*) Surface temperature profiles of evaporating water drops on a glass substrate obtained from finite-element simulations. An inversion in the surface temperature profile occurs as the contact angle changes from $\theta = 10°$ to 15°. (*b*,*c*) Temperature isotherms near the contact line, obtained from an asymptotic analysis, for $\theta = 22.5°$ (geometry not to scale) when (*b*) $k_s/k_l = 10$ and (*c*) $k_s/k_l = 1$. In panel *a*, the isotherms are almost parallel to the drop–substrate interface, indicating that the heat flux is primarily from the substrate to the drop. In panel *b*, the isotherms cross the drop–substrate interface, indicating the presence of radial heat flux in the bulk of the drop. Panel *a* adapted with permission from Reference 71. Panels *b* and *c* adapted with permission from Reference 67.

respectively. In the limit of $k_s \gg k_l$, the substrate temperature will be fairly uniform (**Figure 5*b***). Then, the surface temperature $T - T_\infty$ is determined primarily by the evaporative flux, $J^a(r)$, and the height of the drop, $h(r)$. For very thin drops, the variation in conduction path length [namely $h(r)$] may not be that significant compared with the variation in evaporative flux from the drop surface. In such cases, the large evaporative flux at the contact line cools the edge of the drop much more than the apex, resulting in a temperature decrease from the apex to the contact line (**Figure 5*a***). On the other hand, if the contact angle is sufficiently large, then the apex of the drop is much further from the substrate than the contact line. As a consequence, the heat conducted to the drop surface at the apex may not compensate for the latent heat removed as a result of evaporation as much as it does at the contact line. Therefore, the apex of the drop remains colder than the edge of the drop.

However, if $k_s/k_l < \tan(\theta)\cot[(\theta/2) + (\theta^2/\pi)]$, then the conductive heat transfer in the substrate cannot be neglected, and the substrate–drop interface will not be at a uniform temperature (67). In such cases, the source of heat that compensates for the latent heat of evaporation is primarily the sensible heat of the drop itself. Therefore, a large evaporative flux at the contact line cools the edge of the drop much more than the apex, resulting in a surface temperature that increases from the edge to the apex (**Figure 5*c***). Note that the above estimate of the critical ratio of thermal conductivity at which the temperature profile reverses is derived by analyzing the heat transfer problem in a 2D wedge, an approximate geometry for the contact line region.

4.4. Evaporation-Driven Fluid Flows in Sessile Drops

Evaporation can generate fluid flows inside a sessile drop in two distinct ways: (*a*) radial convection (a direct effect arising from mass conservation) and (*b*) Marangoni flows (an indirect effect arising from an uneven temperature profile on the surface of the drop). For thin drops (small θ), the flow dynamics inside the drop can be analyzed under lubrication approximation. Then, radial velocity that develops inside the drop due to these two effects can be derived in a cylindrical coordinate

system (r, z) (**Figure 4*c***) as follows:

$$u_r = \frac{4J_0R}{\pi\rho_l r\theta(t)}\left(\frac{1}{\sqrt{1-(r/R)^2}} - [1-(r/R)^2]\right)\left[3\frac{z}{h} - \frac{3z^2}{2h^2}\right] - \frac{(-\beta)h}{4\mu}\frac{dT}{dr}\left[3\frac{z^2}{h^2} - 2\frac{z}{h}\right], \quad 4.$$

where ρ_l, β, and μ represent the density, temperature coefficient of the surface tension, and viscosity of the liquid, respectively. In Equation 4, the first and second terms, referred to as u_r^E and u_r^M, respectively, represent the contributions from radial convection and from the Marangoni flow. These flow mechanisms can be understood as described below.

4.4.1. Radial convection. The evaporative flux from the drop surface, given by $J(r)$ in Equation 2, will require the drop to shrink. However, the contact line may not move, since the physical and chemical heterogeneities inherent in the substrate may lead to pinning of the contact line (68). The presence of additives such as colloidal particles (18) and polymers (69) will also enhance the pinning of the contact line. The contact line of the drop can then sustain (i.e., remain at the same location) only if the fluid from the bulk of the drop moves toward the contact line to compensate for the evaporative loss at the contact line. This fluid motion from the center of the drop to the contact line creates a convective flow field in the radial direction inside the drop.

If $u_r^E(r, z)$ is the radial velocity that develops inside the drop, then the height-averaged fluid velocity, $\bar{u}_r^E = 1/[h(r)]\int_0^{h(r)} u_r^E(r, z)dz$, is given by the first term in Equation 4 (19, 33, 64). This height-averaged velocity, $\bar{u}_r^E$, has two interesting features:

1. Spatial divergence. As $r \to R$, $\bar{u}_r^E$ diverges as $1/\sqrt{1-(r/R)^2}$, reflecting the singularity in the evaporative flux at the contact line. For finite but small θ, this divergence is weaker and is approximately of the form $\bar{u}_r^E \sim 1/[1-(r/R)^2]^{(1/2)-(\theta/\pi)}$ (70). In other words, as evaporation proceeds, the rate of change of the drop height $h(r)$ near the contact line is very small, such that the large evaporative flux near the contact line must be compensated for by an equally strong flow from the bulk toward the contact line (**Figure 6*a***). This radial flow drives coffee-ring formation in evaporating sessile drops (18).
2. Temporal divergence. As the drop reaches its lifetime, $t = t_f$, the instantaneous contact angle $\theta(t) \to 0$ and $\bar{u}_r^E$ shows a temporal divergence. For thin drops, the contact angle is a linear function of time, $\theta(t)/\theta(t=0) = 1 - t/t_f$; therefore, the nature of this temporal divergence is $\bar{u}_r^E \sim (t_f - t)^{-1}$. This temporal divergence in the radial flow is responsible for the complete transport of any suspended or dissolved particles in the fluid to the contact line and generates a rush-hour effect (33) (**Figure 6*b***).

Because the radially flowing fluid is confined between the solid substrate and a stress-free interface, it is reasonable to compare the flow field with the Poiseuille flow profile and approximate the height-dependent velocity profile, $u_r^E(r, z)$, as a quadratic function of z (33, 70). Thus, a half-parabola represents the velocity field u_r^E at each radial location r, as evident from the expression in square brackets in the first term of Equation 4. Furthermore, mass conservation demands that the radial flow must be accompanied by an axial flow, $u_z(r, z)$, which can be calculated from the incompressible flow condition $\nabla \cdot \mathbf{u} = 0$, though u_z will be h/R smaller than the radial component for thin drops, as usual in lubrication analysis. However, near the contact line, contributions from u_z may not be always negligible (70).

Thus, the mismatch between the evaporative flux from the surface of the drop and the interface shrinkage rate gives rise to radial convection in the bulk of the drop. This radial flow is often referred to as capillary flow in the literature, though its origin is not associated with any "capillarity" effects. Instead, the flow is a consequence of mass conservation—to compensate for the evaporative loss.

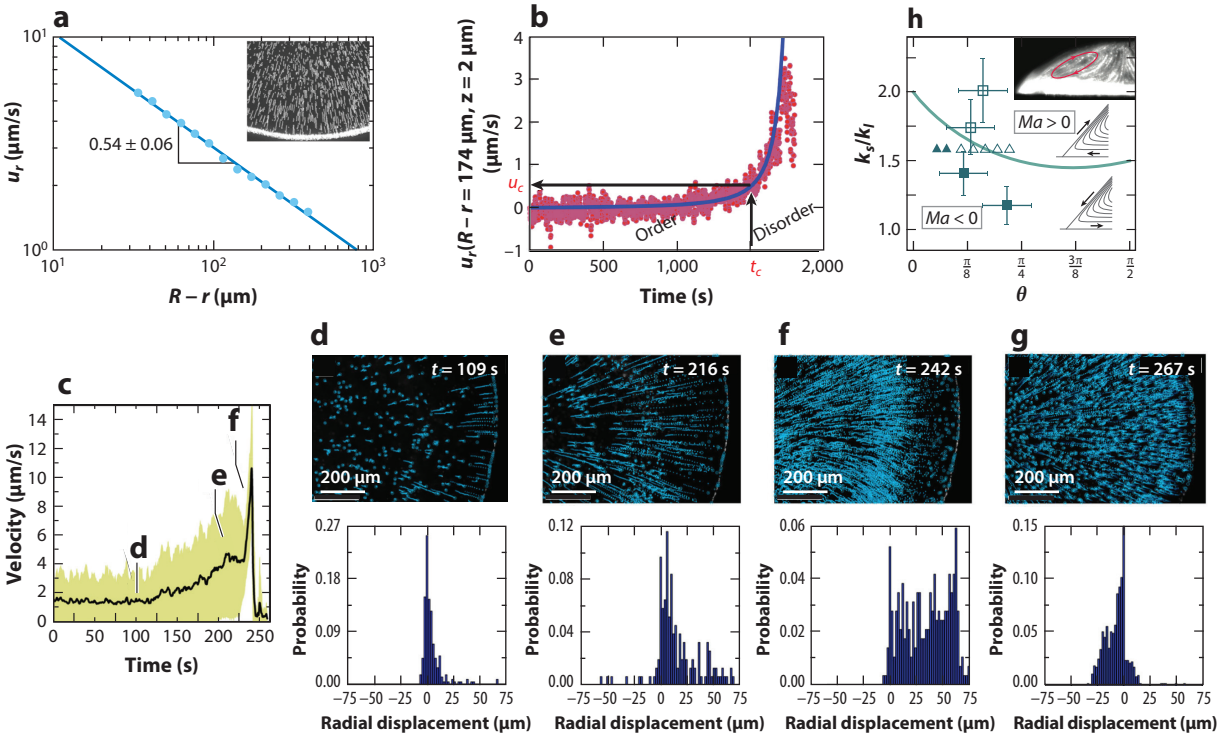

Figure 6

(*a*) Spatial divergence in the velocity field inside an evaporating water drop ($\theta \approx 11.5°$). (*Inset*) Stitched images of microspheres undergoing radial convection. (*b*,*c*) Temporal divergence of the velocity field in an evaporating aqueous drop containing polystyrene particles measured at (*b*) 2 μm and (*c*) 4 μm above the substrate. (*d–f*) (*top*) Particle trajectories over 25 s and (*bottom*) histograms of radial displacements over 5 s at different instances of time corresponding to panel *c*. (*g*) Marangoni stress–driven inward flow revealed by particle trajectories and histograms of radial displacements (negative, unlike the displacements in panels *d–f*) of polyvinyl alcohol–modified fluorescent polystyrene particles. (*h*) Dependence of the flow direction on the thermal conductivities of the medium and contact angle. The squares correspond to drops of chloroform, isopropanol, ethanol, and methanol evaporating on polydimethylsiloxane. Triangles represent numerical calculations in Reference 71. Open symbols represent fluid flow away from the contact line along the drop surface, indicating $Ma > 0$, and filled symbols represent flow toward the contact line, indicating $Ma < 0$. The continuous line is a theoretical prediction based on an asymptotic analysis. (*Inset*) Visualization of flow using fluorescent particles in an evaporating octane drop, corresponding to $Ma = 45{,}800$ (only half of the drop is shown). Panel *a* and its inset adapted with permission from References 19 and 18, respectively. Panel *b* adapted with permission from Reference 33. Panel *c* adapted with permission from Reference 39. Panel *g* adapted with permission from Reference 39. Panel *h* adapted with permission from Reference 67.

4.4.2. Marangoni flows. As discussed in Section 4.3, evaporation generates a nonuniform temperature distribution in the sessile drop. The variation of temperature at the drop surface is particularly interesting because surface tension is a function of temperature. For most liquids, surface tension decreases with an increase in temperature. This dependence can be quantified using the temperature coefficient of surface tension, defined as $\beta = d\sigma/dT$, where σ is the surface tension. For water, $\beta = -0.15$ mN/mK (72). This surface tension gradient ($\nabla\sigma$) must be balanced by tangential viscous stress at the drop surface, implying that a fluid flow must develop in the drop bulk, in addition to the radial convection.

The exact nature of the Marangoni flow depends on the local surface tension gradient, which in turn depends on the surface temperature profile. As discussed above, the nature of the temperature profile itself depends on the thermal conductivity of the substrate, on that of the drop,

and on the instantaneous drop shape (or, equivalently, the contact angle). The second term in Equation 4 describes the Marangoni flow generated due to the surface tension gradient. Again, the term in the square brackets shows the parabolic nature of the velocity field $u_r^M(r, z)$ in the z direction, while the prefactor can be inferred as the height-averaged velocity $\bar{u}_r^M$. If the temperature is cooler at the apex than that at the edge ($dT/dr > 0$), then $\bar{u}_r^M$ is negative in the entire thickness of the drop ($0 < z < h$). In other words, the greater surface tension at the apex of the drop draws fluid toward it along the interface. This flow is in the opposite direction of radial convection; thus, it may diminish or completely suppress the latter. On the other hand, if the apex is warmer ($dT/dr < 0$), then $\bar{u}_r^M$ is positive. In this case, the greater surface tension at the edge of the drop drives fluid flows toward the edge, enhancing the radial convection (**Figure 6*c***).

The strength of the Marangoni flow can be deduced by nondimensionalizing $\bar{u}_r^M$ with R/t_f, T with ΔT (where ΔT is the difference in temperature between the edge and the apex), and r with R. Then, the second term in Equation 4, u_r^M, becomes proportional to the Marangoni number (35), defined as $Ma = (-\beta \Delta T t_f)/\mu R$. A large positive Marangoni number indicates a strong recirculatory flow against the radial flows, whereas a negative Marangoni number indicates a Marangoni flow that adds to the radial flow. Consider a typical scenario where a sessile water droplet of $R = 1$ mm evaporates in 10 min. A surface temperature difference of $\Delta T = 0.01$°C gives $Ma = 1{,}000$. Therefore, a small difference in the surface temperature can result in Marangoni flows that may enhance or diminish the radial convection (**Figure 6*c–b***). Clearly, Marangoni flows can be significantly dominant when evaporation occurs on heated substrates.

When surface-active polymers or surfactant molecules are present in a drop, they get adsorbed to the drop surface. However, the convective flows described above alter the surface concentration of surfactants, resulting in surface tension gradients—yet another source of Marangoni flow. This solutal Marangoni flow, generated by surface-active species, can completely suppress the convective flows or reverse the flow field itself (37, 71–73). In fact, surface contaminants as small as 300 molecules/μm^2 can completely suppress thermal Marangoni flow in evaporating water droplets (35). Similarly, in evaporating binary fluid drops, the difference in volatility leads to differential evaporation of the components, creating Marangoni-driven internal flows (74, 75). On the other hand, when colloidal particles are present in a drop, they can get adsorbed onto the drop–air interface. This particle-laden interface increases both the surface viscosity (42) and the elasticity (31) of the interface, deforms the interface (76), and can weaken or even inhibit the Marangoni flow and the radial convection (42, 77). Thus, in such cases, the drying drop leaves behind a uniform deposit, instead of a coffee-ring pattern.

4.5. Numerical Simulations

Drying drops of colloidal dispersions encompass heat, mass, and momentum transport processes, spanning molecular, mesoscopic, and macroscopic length scales. Therefore, computer simulations that simultaneously capture all relevant physical phenomena in a drying drop are difficult. Most numerical studies, therefore, have focused on specific physics to explain experimental observations. Several of these studies used Equation 4 to describe the flow field inside an evaporating drop and investigate the trajectory and fate of the suspended particles in conjunction with other methods, such as Monte Carlo simulations (78) and discrete-element models (77). Such studies often neglect changes in vapor diffusion and flow fields caused by changes in the geometry of the system, hydrodynamic interactions between suspended particles, spatial and temporal heterogeneity in the physical properties of the dispersion that develop in the drop as a result of the redistribution of suspended particles, detailed heat transport mechanisms, changes in drop shape, elasticity of the interface due to the adsorption of particles, and so forth. Therefore, a generic computational tool

to simulate the evaporation of drops of colloidal dispersions will contribute significantly to the growth of this field.

5. TRANSPORT IN EVAPORATING PARTICLE-LADEN DROPS

Particles in an evaporating drop can be transported as a result of various types of flows generated within the drop. In addition, interface-mediated transport may occur, especially if the particles are adsorbed to the liquid–air interface. Therefore, in general, particle transport is influenced by (*a*) the factors that govern the rate of evaporation, such as the temperature of the substrate and of the surroundings, the thermal conductivity of the substrate, the volatility of the solvent, and humidity, and (*b*) the presence of additives such as surfactants, polymers, or other species along with the particles. These additives can adsorb to the interface and can affect both flow within the drop and flow along the interface.

5.1. Flow-Mediated Particle Deposition

A coffee ring forms when the radial convective flow carries the dispersed colloidal particles in the drop to the contact line and deposits them. The temporal divergence of the radial convection can significantly affect the particle deposition process and hence the final pattern. Marangoni flows also advect the dispersed particles. As discussed above, the sense of direction of the Marangoni circulations is determined by the ratio of the thermal conductivity of the liquid to that of the substrate; however, experiments (67) have shown that, irrespective of the sense of circulation, the dispersed particles are deposited mostly at the stagnation points near the liquid–air or solid–liquid interface. Thus, regardless of the direction, Marangoni flows always destroy the edge deposition (coffee ring). However, because the flows are at a low Reynolds number, the dispersed particles must continue to be part of the circulatory flows. The reason for their rejection (escape) from the circulations and their deposition near the stagnation points is not clear.

For the fluid flows and the particle deposition processes discussed above, we have assumed that the contact line remains pinned onto the substrate. Contact line pinning in a drying drop is a self-enhancing effect because the deposited particles pin the contact line (79), which is necessary for the development and strengthening of radial convective flow. If the contact line is not pinned, it drifts inward as drop evaporation proceeds. This inward motion reduces the strength of the radial convection because (*a*) inward movement of the contact line competes with the radial flow and (*b*) the larger contact angles reduce the strength of divergence of the evaporative flux at the contact line. Thus, particle deposition does not occur exclusively near the contact line. Instead, it occurs over a region close to the center of the drop, leading to mountain-like deposits, or at intermediate radii, leading to volcano-like deposits (52). Therefore, the exact nature of the deposit left behind by a drying drop of colloidal dispersion depends on both the kinetics of evaporation and the depinning dynamics (and the associated timescale) of the contact line.

5.2. Interface-Mediated Particle Deposition

Another mechanism that has attracted increased attention is interface-mediated particle transport (28, 32, 39, 42). The adsorption of particles to the drop surface or the drop–air interface is favored when the particles in the drop are surface active. The particles can also be adsorbed if the interface shrinks at a rate faster than the diffusion of the particles (42). The adsorbed particles cause changes in the interfacial tension. Nonspherical particles adsorbed on the interface even form clusters, significantly increasing the elasticity of the interface (36). The adsorbed particles are not carried to the edge by the convective flows; therefore, uniform deposit of particles results when the adsorbed particles are deposited at the substrate at the end of the evaporation process (42, 77). If particle

adsorption is suppressed (say, by slow evaporation), then coffee-ring formation occurs as a result of the dominant outward flow inside the drying drop.

6. EVAPORATING SESSILE DROPS OF COMPLEX FLUIDS

Evaporation of pure liquid drops has received significant attention since the early twentieth century (63). Interesting physics of internal fluid convection and subsequent pattern formation from drying drops have been revealed as these research efforts widened to study colloidal dispersions. The focus of these recent efforts has slowly shifted to the drying of different types of complex fluids, the topic of this section. Because the drying of drops of colloidal dispersions without additives is discussed above, we focus here on other complex fluids.

6.1. Surfactant Solutions

The presence of surfactants in colloidal dispersions, either added externally or autoproduced by dispersed particles such as bacteria (47), influences the evaporation process in a drop in multiple ways. First, because surfactants are invariably adsorbed to the drop surface, thereby reducing interfacial tension, the wettability of the drop on the substrate is enhanced. Thus, a longer spreading process is often observed upon placing a surfactant-laden drop on a substrate. As the drop dries, the concentration of the surfactants in the drop increases, implying that the drop on the substrate experiences variations in wettability as it evaporates. This leads to a multistage evaporation process in comparison to the evaporation of pure liquids (80, 81). Second, the adsorbed surfactants at the liquid–air interface generate Marangoni vortices, as described in Section 4.4.2. These counterflows reduce the ring deposit or even yield a central deposit (47). Third, the reduced surface tension of the drop–air interface reduces the pinning force. Therefore, an evaporating drop containing surfactants may easily depin, affecting the evaporation process (82). The continuous depinning of the contact line typically yields a uniform deposit. Fourth, if the surfactants are long-chain molecules like polymers—say, molecules like polyethylene glycol (PEG)—then they can increase the viscosity of the drop fluid. This enhanced viscosity then suppresses the radial flows, resulting in less deposition in the ring (82). Therefore, the presence of surfactant molecules can retard or suppress the coffee-ring effect in evaporating drops via multiple mechanisms.

6.2. Polymer Solutions

The addition of polymers can affect pattern formation in multiple ways (69). Typically, polymers induce depletion interactions between the colloidal particles, causing colloidal clusters to form. If these clusters are large, they are less affected by the fluid flows generated inside the evaporating drop; therefore, the coffee-ring effect is usually suppressed following the addition of polymers. On the other hand, if the colloids are large enough (10 μm), then the depletion interactions are weak. Thus, larger colloids are susceptible to radial convection, even if polymers are present, and may show distinct coffee-ring formation.

Interestingly, some polymers can enhance pinning of the contact line. Thus, depinning of the contact line at the end of rush hour is delayed, inducing higher velocities inside the evaporating drop. This flow can drive particles to the contact line even if they had already formed clusters due to depletion interactions with polymers.

Another strategy to exploit the properties of polymer in drop-drying problems, particularly for coffee-ring suppression, is to have high-molecular-weight (long) polymers physisorb onto the surface of the colloidal particles. The main challenge is to maneuver the right number of polymers and particles so that the physisorbed particles are fully captured on the descending interface of the drop (with no excess particles or polymers in the bulk). This technique allows

one to ensure coffee-ring suppression to the extent that the resulting deposit will be much more uniform than when other methods are used, such as with the addition of surfactants (39). Due to steric repulsion, the physisorbed particles do not aggregate on the interface. Moreover, the presence of thermal Marangoni flows, if toward the apex, can counter the deposition of particles near the contact line. If the particle concentration in the drop is in the right range—just sufficient to cover the drop–air interface—then the particles will be deposited onto the substrate surface as a uniform deposit upon complete evaporation of the solvent. A similar way to obtain uniform deposits using microgel particles has recently been proposed (83).

Experiments (36) have shown that coffee-ring formation can be suppressed using anisotropic particles (see Section 6.5, below). However, the uniform deposits generated by drying of drops containing polymer-adsorbed spherical colloids (39) show that the mechanism at work is not the particle shape anisotropy but the process of interfacial adsorption followed by direct deposition. Further careful studies are required to settle this issue. Thus, the role of particle shape in the presence and absence of polymers, the configurational state of the physisorbed polymer chains, and the differences that may arise if the polymer chains are grafted onto the polymers are issues requiring further investigation.

6.3. Dissolved Solids

Water, a natural substance used in all applications, often contains salt and other dissolved materials. When drops of salt solution (43, 84, 85), sucrose, glucose, fructose (44), and so forth are dried, the higher evaporative flux will cause supersaturation to occur near the contact line and the first crystals will form near the contact line. Nucleation may occur at the liquid–air interface or at the solid–liquid interface in the vicinity of the contact line. The newly formed crystals can remain anchored or be pushed inward by the dynamics of the interface (86). Thus, the final patterns obtained depend on the location of the nucleation site, the growth dynamics, and the fluid dynamics in the evaporating drop.

Unlike particles, crystallized salt near the contact line is generally less capable of pinning the contact line (43, 44). Therefore, drop evaporation may proceed with either continuous or discontinuous depinning of the contact line, causing the radial convection in the drop to weaken. Thus, a uniform deposit or concentric rings may be obtained instead of a coffee ring. On the other hand, a coffee-ring pattern can be obtained through the addition of colloidal particles to the solutions, which will pin the contact line (43). Furthermore, the crystallized dissolved species may develop their own characteristics, for example, interesting crystal morphology (86) and dendrite patterns (43). The deposit patterns can also be tuned to obtain concentric rings or a spiral-like morphology by adjusting the evaporation rate (87).

6.4. Binary and Ternary Mixtures and Emulsions

When the evaporating drop is a liquid mixture, a multitude of features emerge because the volatility of each constituent is different. As a result, the concentration of the mixture and hence the physical properties of the drop, such as density, viscosity, and surface tension, vary as the drop evaporates. Moreover, the concentration of the liquid mixture varies spatially inside the drop because the evaporative flux is inhomogeneous on the surface of an evaporating drop (discussed in Section 4.2). The most appealing effects of the spatial variations in concentration are the development of surface tension gradients and the resulting (solutal) Marangoni flows, which substantially affect pattern formation if the liquid mixture contains nonvolatile components such as colloidal particles or polymers. The relative volatility between different components of the liquid mixture may also result in phase separation of the constituents as evaporation

proceeds. Therefore, it is desirable to categorize the evaporation of liquid mixtures as either (*a*) multicomponent, single-phase liquid mixture drops or (*b*) multicomponent, multiphase liquid mixture drops. In the former, the components remain miscible throughout the evaporation, whereas in the latter, phase separation may occur during the process of evaporation.

Multicomponent, single-phase liquid mixtures have been studied primarily with the aim of suppressing coffee-ring formation in different applications such as inkjet printing. Consider the evaporation of a binary drop (containing two liquids) deposited on a solid substrate. Typically, after capillary spreading of the drop, the contact line remains pinned (CCR mode) as the drop evaporates, with the highest flux near the contact line. Therefore, in the neighborhood of the contact line, the concentration of the less volatile component increases with time. Two different scenarios may result. On one hand, if the less volatile component has more surface tension, a positive gradient in surface tension toward the contact line develops as drop evaporation proceeds. Consequently, liquid flows toward the contact line, resulting in further (Marangoni stress–driven) spreading of the drop. As a result, the contact line does not remain pinned; instead, the drop continues to spread even while it is evaporating (88). This mode of evaporation is very different from the CCR, CCA, and mixed modes of evaporation that single-component liquids exhibit. Due to Marangoni spreading, the resulting shape of the binary fluid drops is pancake-like (88). For very small (picoliter-volume) drops, even when the contact line is pinned, the Marangoni flows can be so strong that they maintain the pancake shape of the drop (dominating the effects of surface tension to maintain a spherical cap shape) (89). These drops appear similar to gravity-deformed puddles, although gravity has no role in dictating the drop shape. In such pancake-shaped drops, the singularity in the evaporative flux at the contact line is not prominent; therefore, the radial convective flows are weak, such that they do not carry dispersed particles, if any, to the contact line. Thus, solutal Marangoni flows directed away from the contact line can suppress the coffee-ring effect, as has been demonstrated experimentally (88, 89).

On the other hand, if the less volatile component has less surface tension, then the differential evaporation and resulting Marangoni flows drive the fluid toward the apex of the drop. These flows will also suppress the coffee-ring effect if the drop contains dispersed particles.

Drying drops of emulsions are an example of a multicomponent, multiphase system. For example, when oil-in-water or water-in-oil emulsions are dried (90, 91), evaporation-driven flows carry the dispersed droplets to the periphery of the evaporating drop, bringing them close to one another and thus facilitating drop–drop coalescence. On one hand, on a hydrophobic surface, the coalesced oil droplets form an oil layer that spreads beyond the initial contact radius. When that happens, there will be an aqueous drop in the center surrounded by an oil layer. When it dries, this aqueous drop can leave deposits of the dispersed entities, such as surfactants, if any were present in the aqueous medium. Such deposits will appear as a central deposit at the end of the drying process. On the other hand, on a hydrophilic surface, an aqueous layer forms outside the oil layer. Evaporation of this aqueous layer, which is depleted of oil, will deposit any dispersed content onto the substrate, generating a pattern similar to the coffee ring. Thus, the wetting characteristics of the substrate dictate the pattern formed by drying drops of emulsions. Although the effect of wettability seems similar to that of solid-particle dispersions, the mechanisms that generate the patterns are different for emulsions.

Multicomponent, multiphase drop-drying scenarios also present interesting possibilities, for example, as a potential model system that mimics prebiotic compartmentalization (92, 93). Consider an aqueous sessile droplet containing a homogeneous mixture of neutral polymers such as dextran and PEG. As drop drying proceeds, the concentration of the polymers in the drop increases, making the polymer solution undergo liquid–liquid phase separation. The nuclei may grow as distinct droplets, or they may coalesce to form a continuous structure. Either way, the

growth of the phase-separated liquid occurs from the contact line region into the bulk of the drop, because the highest evaporation flux is at the contact line and, therefore, phase separation will be initiated in the neighborhood of the contact line. Also, a high concentration of polymers near the contact line reduces the local surface tension, inducing Marangoni flows that help the polymers propagate away from the contact line. These phase-separated mixtures illustrate a potential mechanism for the formation of prebiotic compartmentalization without membranes that may act as storage and transcription for nucleic acids (92).

Complex suspensions made of a mixture of emulsion droplets and colloidal particles represent still another multiphase, multicomponent system (94). In such systems, toward the end of drying, air invades the jam-packed particle–emulsion structure. The invading air can break the large emulsion droplets but not the smaller ones, since the latter resist breakup. The large droplets that are broken are pushed aside into a porous structure formed by the particles. Therefore, the resulting deposit will have two types of pores: (*a*) pores dictated by closely packed particles in air and (*b*) larger gaps that result from deformed emulsion droplets. Thus, drying complex suspensions can be used to make hierarchical porous structures.

6.5. Anisotropic Constituents

Drying drops with anisotropic constituents dispersed in a solvent can be classified into two categories: (*a*) solutions of long-chain molecules such as chromonic liquid crystals, protein molecules, and DNA and (*b*) suspensions of colloidal particles with shape anisotropy such as ellipsoids, rods, or discs. A feature that arises in such systems is the development of orientational order in the drop, either during evaporation or when molecules or particles are deposited after the drying process is complete.

In the usual case, where convective flows are primarily radial, the elongated constituents will be flow aligned and retain their orientation as they are deposited, as observed in the case of DNA (95), collagen fibers (96), and silica rods (34). The ordered structures in the deposit can develop distinctive attributes that can be useful in tissue engineering and developmental biology. For example, the ordered deposits of DNA show wrinkling instabilities and generate zigzag patterns (95). Similarly, when drops containing cells and type I collagen (a self-assembling protein) are dried, the aligned collagen network influences the behavior and differentiation of cells. In such cases, leaving the evaporation incomplete will produce cell-laden hydrogels as the end product.

However, the alignment of anisotropic entities in the deposit may differ or be completely lost if other factors, such as interface phenomena, surface or bulk elasticity, thermal diffusion, or intrinsic phase transitions, compete with convective flows. A study using chromonic liquid crystals (76) presents an example of the last factor, phase transitions. Chromonic liquid crystals exhibit isotropic, nematic, or columnar phases with an increase in concentration. Therefore, during the drying of a drop containing chromonic liquid crystals, temporal and spatial variations in the concentration lead to the emergence of different phases (76). If drop drying proceeds slowly, the anisotropic constituents have sufficient time to relax, generating a uniform orientational order in the drop. On the other hand, the phases may get kinetically trapped in the case of fast evaporation, as different phases are deposited onto the substrate without further rearrangement. Thus, system-specific phase transitions and the resulting effects (e.g., variation in surface and transport properties), occurrence of defects, and grain boundaries separating various phases in the deposits can be observed when drops containing anisotropic particles are dried.

When adsorbed, anisotropic colloidal particles can dramatically enhance the elasticity of the liquid–air interface. The underlying reason is that interfacial deformation due to the presence of a nonspherical particle is typically greater than for a spherical particle. Therefore, capillary attraction between nonspherical colloidal particles is stronger than that between spherical particles,

restricting the dynamics of the adsorbed particles on the interface. This increased elasticity of the interface can suppress the coffee-ring effect in two different ways. First, the increased elasticity is so large that radial convection flows are completely suppressed inside an evaporating drop, and the coffee-ring effect vanishes (36). Second, the higher energy cost of adsorption makes the depinning of an anisotropic particle–laden interface easier compared with a spherical particle–laden interface, leading to a uniform deposit (97). However, it is not clear whether both mechanisms are simultaneously at play—a point to be addressed theoretically.

Other studies have demonstrated that deposit patterns are altered not only by a change in the aspect ratio of the ellipsoids but also by (*a*) competition between capillary interactions that dictate assembly of ellipsoids at the drop surface and migration of particles to the contact line as a result of evaporation (98) and (*b*) particle–particle and particle–substrate interactions (31). Colloidal rods in coffee stains obtained by drop drying have been observed to exhibit an order–disorder transition similar to that observed in deposits of spheres (34).

6.6. Biological Fluids

Research on patterns resulting from the drying of several complex biological liquids (e.g., blood, synovial fluid, urine, serum) extracted from animals is fast expanding and has attracted considerable interest (99–106). The analysis and interpretation of patterns of dried biological fluids can provide a rapid homegrown means to identify disease conditions. For example, a comparison of the deposit patterns formed by the evaporation of sessile drops of blood extracted from a healthy individual and from a person with disease can provide morphological features that can be used to make inferences about disease conditions (102).

Drops of synovial fluid (a complex fluid in the cavities of synovial joints) dried on microscopy slides have revealed chemical changes associated with osteoarthritis. The content and secondary structure of proteins in the dried deposit patterns of patients' synovial fluid, analyzed by Raman spectroscopy, have been used to detect the extent of knee damage due to osteoarthritis (103, 104). Similarly, the evaporation of urine drops on superhydrophobic surfaces is a low-cost tool for detecting preeclampsia in pregnant women. Because the concentration of protein in the drop increases during evaporation, such methods offer improved sensitivity in detection limits (105).

Although the patterns that form when biological fluids are dried are reproducible across tests to some extent, the mechanism of pattern formation and analysis of the microstructure continue to be challenging as a result of issues such as varying composition. It is important to take this fact into account when such approaches are proposed as simple and rapid diagnosis tools.

6.7. Active Fluids

Unique nonequilibrium features associated with the dynamics of active fluids have recently sparked interest within the research community. However, the role of drying in drops of active fluids has been less well explored.

Active fluids are typically constituted by "living" particles that consume energy from the local environment and convert it into mechanical motion. Thus, active fluids are intrinsically out of equilibrium. In the case of drying drops, evaporation imposes internal convection; therefore, drying drops of active fluids constitute an ideal model system to study the competition between intrinsic (activity-driven) and imposed (drying-driven) nonequilibrium features in a single system (107). This competition leads to changes in, for example, the growth dynamics of the deposit. In drying drops containing *Pseudomonas aeruginosa*, activity manifests as the production of biosurfactants. The adsorption of biosurfactants to the drop interface leads to solutal Marangoni

flows, which compete with radial convection. Therefore, oscillatory flows are generated and the coffee-ring effect is suppressed in the final patterns (47).

The microscopic activity of bacterial cells often leads to collective cellular motion, which produces a local orientational order of the bacteria inside the drop similar to that of the anisotropic constituents discussed in Section 6.5. This order can give rise to different instabilities in the deposits (108) and in the final patterns (109). Such studies are also expected to yield insight into active self-assembly, biofilm formation, and pathogen spreading.

7. DRYING IN COMPLEX CONFIGURATIONS

As discussed in this review, evaporation of sessile drops of pure fluids and of sessile drops containing colloidal particles have been extensively studied. An emerging area that naturally follows these studies is drying of drops in more-complex configurations, such as (*a*) in confinement, (*b*) on patterned surfaces, (*c*) with differential heating, and (*d*) on inclined substrates.

7.1. Drops Drying in Confinement

Given that the evaporation of a drop drives the transport phenomena within it, it is not surprising that patterns can be tuned by altering the evaporation process. One such possibility is placing the drop in a confined environment, that is, between a substrate and another surface over the drop. Different variations of the overhead surface have been analyzed: (*a*) The surface may partially or fully cover the drop (i.e., the projected area of the overhead surface may be smaller than or equal to the projected area of the drop); (*b*) it may be a flat, inclined, or curved surface; (*c*) it may or may not be in contact with the drop interface; or (*d*) the confining surfaces may have different physicochemical properties. Depending on the configuration and the materials used, different patterns can be obtained.

The presence of an overhead surface on a drop residing on another substrate reduces the area available for evaporation. If the internal flows are weak and the surface tension effects are slow to act, then the deposited film can have nonuniform thickness, thereby imprinting the signature of the overhead surface (mask) (110). If the overhead surface has holes, then the holes will allow unhindered evaporation in certain regions of the drop or film while evaporation from the rest of the region remains hindered. Higher evaporation rates from the drop or film surface drive flows toward the holes, concentrating the particles near such regions. A patterned network of nanoparticle–microparticle assemblies was obtained with a binary dispersion through the use of this technique (111). However, it is not clear whether the accumulation of particles below the holes on the mask starts at the beginning of the experiment or at later stages. Further studies are needed to determine the individual roles of particle size and concentration as well as the sizes and shapes of the holes on the overhead surface.

Several configurations, such as sphere-on-plate, parallel-plate, cylindrical confinement, and wedge-shaped geometries, have been used to study the evaporation of polymer solutions and particle-laden fluids that are initially in contact with the confining surface. When drops dry in these configurations, their pinning behavior is modified, resulting in interesting patterns such as concentric rings, spirals, and scallop shells (57, 61, 112–114). Spiral patterns form over a wide range of spacings (~90–190 μm) between parallel plates (**Figure 7*a–c***). Such patterns result regardless of the shape of the particles in the colloidal dispersion as the three-phase contact line undergoes continuous stick–slip motion. Patterns with multiple rings (**Figure 7*d–f***) seem to be characteristic of the sphere-on-plate geometry, wherein the curved surface of the sphere constitutes the overhead surface while the drop is deposited onto the plate (57, 112, 114). As the liquid evaporates, the contact line continuously slips on both surfaces. Experiments have shown that the

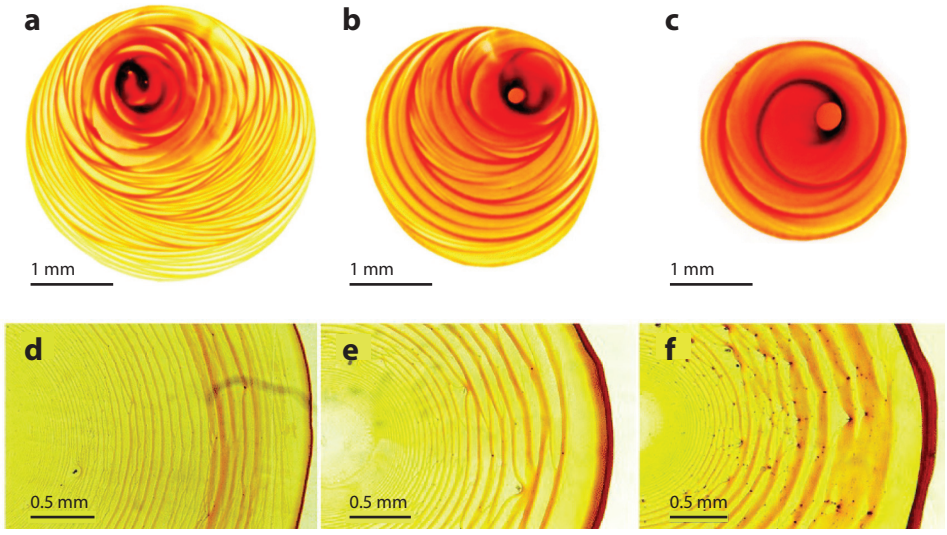

Figure 7

Characteristic spirals and multiring deposits formed by drying colloidal dispersions containing hematite ellipsoids in (*a–c*) parallel-plate confinement and (*d–f*) a sphere-on-plate configuration. The initial concentration of the particles in the dispersions used to generate the dried patterns shown in panels *a–c* is 3 wt%, and the spacing between the parallel plates is (*a*) 93 μm, (*b*) 137 μm, and (*c*) 186 μm. The initial concentrations of particles in the dispersions used to generate the dried patterns shown in panels *d–f* are (*d*) 0.12 wt%, (*e*) 0.30 wt%, and (*f*) 0.5 wt%. Panels *a–c* adapted with permission from Reference 61. Panels *d–f* adapted with permission from Reference 57.

pinning force is dictated by the initial concentration of particles, which is reflected as a change in the frequency of depinning events as the concentration is varied (112). The reason for the slip is not clear, but the capillary force may drive the shrinking contact line while the pinning force opposes the tendency of the drop to satisfy Laplace's and Young's laws.

In the case of an evaporating sessile drop, the pinning force typically dominates the capillary force, resulting in a single ring. However, in confined drops, the capillary force can dominate the pinning force (multiple times), possibly because the drop confined between the surfaces has greater curvature. However, further numerical and theoretical investigations are required to support this argument.

The convective patterns generated inside the confined drop have not been examined, but this aspect is likely to be interesting for several reasons. First, the nonuniform flux on the drop surface is crucial in establishing the flows inside the sessile drop. However, in a confined drop, the area available for evaporation is restricted, raising the question of the extent to which inhomogeneous evaporative flux can induce fluid flows. Second, Marangoni flows are suppressed by the presence of the solid surface if it is in contact with the evaporating drop; therefore, in such systems the contribution of surface tension gradient–driven flows is likely to be weaker. However, these issues have not been studied.

The evaporation of drops in confined environments is an emerging field, and future investigations should focus on addressing the questions raised above. It may also be interesting to note that the nonparallel geometry of confinement manifests in the details of the final pattern left behind on the plate. For example, in the case of concentric rings, (*a*) the height of the deposit at different radial locations is not the same but rather varies among rings, and (*b*) the distance

between consecutive rings does not remain constant when drop drying occurs in a sphere-on-plate geometry.

7.2. Drops Drying on Patterned Surfaces

Surface patterning plays a role in evaporating drops because topographical and chemical defects, whether regular or irregular, affect the motion of the contact line during evaporation. Typically, on regular, unpatterned surfaces the inherent irregularities on the surface pin the contact line during most of the evaporation process, leading to the CCR mode of evaporation. However, if the surface roughness is low, the drop continuously depins, leading to the CCA mode of evaporation. Since the mode of evaporation (whether CCR, CCA, or mixed) is usually unpredictable, it is desirable to gain control over the movement of the receding contact line.

To this end, one possibility is to use surfaces that have a well-defined topography but are also sufficiently rough to be impregnated with a lubricant. The former quality ensures the desired predictable pinning events and locations as the drop accesses minima in the free energy landscape, while the latter ensures the desired slip during movement of the contact line (i.e., snap events), allowing stick–slip motion of the contact line to be obtained in a formularized fashion (115). However, whether the dispersed particles (if any) in the drop will affect the stick–slip motion of the contact line on these topographical surfaces has yet to be investigated. The ability to control the spatial distribution of particles by manipulating the dynamics of the contact line when drops are dried on microstructured surfaces has been proposed as an effective strategy to mitigate indirect transmission of infectious disease via, for example, deposition and drying of respiratory drops (116).

Similarly, studies have investigated drop drying on porous substrates, using the structure of the porous media to construct large-scale networks. In this context, the liquid bridges formed in the interstices of the porous media have been exploited to obtain a connected network of particles upon evaporation. Researchers have constructed gold wire networks of different topologies, of centimeter length scales, by drying gold nanoparticle suspensions on 2D crystals of latex particles (117).

7.3. Local Heating of Drying Drops

Differential evaporation from the surface of a drying sessile drop, the main cause of evaporation-driven internal flows, eventually manifests as deposit patterns of various morphologies. Therefore, it is natural to perturb the evaporation rate and investigate the consequences. One way to do so is by heating the apex of the drop with a laser beam, which generates flows toward the apex because (*a*) evaporation is enhanced at the apex (118) and (*b*) buoyancy forces come into play (119). The coffee ring does not form; instead, a central deposition occurs. Furthermore, experiments using drops with fluorescent double-stranded DNA showed that the drop continuously depins upon heating of the apex (118). In other words, drop evaporation occurs in CCA mode and not in CCR mode, which may, again, be a consequence of the reversed flow field. More importantly, this continuous depinning of the contact line also assists in central deposition. The use of laser-induced hydrothermal flows to control particle deposition at colloidal length scales is termed optically directed assembly (119). In contrast, instead of heating the apex, if the entire substrate is heated, the overall evaporation rate may increase, but the characteristics of the internal flows (as discussed in Section 4.3), and therefore the deposit patterns, will remain the same. The drying of gold nanoparticle dispersion drops, when illuminated with a 532-nm laser at the drop apex, creates Marangoni flows owing to the plasmonic effect, leaving coffee-eye-like deposits after complete evaporation of the solvent. The possibility of achieving deposit patterns of various morphologies has been demonstrated via changes in the illumination conditions (120).

7.4. Drops Drying on Inclined Substrates

A detailed discussion of the role of gravity in pattern formation of drying drops can be found elsewhere (62). Experiments on drying water drops on inclined substrates have revealed that the total time of evaporation, also called the lifetime of the drop, is a nonmonotonic function of substrate inclination. The longest lifetime occurs when drops rest on a vertical substrate (90° orientation) as the substrate inclination is changed from 0° to 180° (121). When on an inclined substrate, drops can distort because of gravity; therefore, they are characterized by advancing and receding contact angles (122, 123). This distortion changes the drop surface area available for evaporation. In addition, depending on the drop volume and substrate properties, the pinning of the contact line can be affected by substrate inclination. These aspects can significantly influence the rate of liquid loss from drops on an inclined substrate, in turn affecting evaporation-driven flows and thus the distribution of particles in the dried deposits.

In the case of particle-laden drops placed on an inclined substrate, gravity can affect pattern formation in two different ways—either directly, by inducing a buoyancy force on the particles, or indirectly, by deforming the shape of the drop. In addition, the inclination of the substrate can modify fluid flow inside the evaporating drop (124). An uneven distribution of particles in the coffee stains (e.g., the asymmetric patterns shown in **Figure 3*e***) is one of the most common features reported when drops are dried on substrates oriented at different angles (28, 53–55). Asymmetric coffee stains form when drops containing spherical particles of different sizes (60 nm to 3 μm in diameter), ellipsoidal particles, and rodlike particles are dried on substrates at various inclinations (28, 54, 55). Naturally, the anisotropy in the distribution of particles disappears and a coffee-ring pattern forms when the size of the drops is of the order of nanoliters (i.e., when the drops are too small to be affected by gravity) (54). Although more particles can be concentrated at the receding or advancing side of the deposit, depending on the pinning/depinning dynamics of the contact line (53), recent results have unambiguously demonstrated that more particles accumulate at the lower part or advancing side of the pattern (28, 54, 55).

Different mechanisms have been put forward to explain the asymmetric deposition of particles formed on inclined substrates. These include curvature-driven interfacial particle transport (28), splitting or breakup of the drop at the final stage of the evaporation process (54), and an interplay among different contributions to the velocity of particles (55). On the theory and simulation front, investigators have developed analytical and numerical tools to estimate drop deformation, a model based on lubrication theory for thin drops, and a numerical strategy that aims to understand the influence of various parameters on patterns when drops are dried on oriented substrates (53, 125–127).

8. CONCLUSIONS AND PERSPECTIVES

Drying drops of liquids exhibit rich and interesting dynamics. Despite the hierarchy of the phenomena involved, the main force that drives the nonequilibrium processes in the system is evaporation that occurs as a result of a rather nontrivial aspect, namely the shape of the drop. The dynamics become richer when the drops contain dispersed entities such as colloidal particles of spherical or nonspherical shapes, miscible or immiscible fluids, living organisms or synthetic active particles, biological material such as DNA and blood cells, salts and sugars, surface-active agents such as surfactants, or polymers. A variety of features emerge from an evaporating drop because the associated processes span various phenomena at different length and timescales. For example, heat, mass, and momentum transfer processes create temperature, concentration, and velocity fields in and around the evaporating drop. Interfacial phenomena, such as the mechanics of the three-phase contact line, dictate the geometry of the drying drop and the mode of evaporation.

The collective dynamics, transport, and fate of the dispersed entities are determined by colloidal processes such as electrostatic- and wettability-triggered interactions between these entities or the interactions of the entities with the solid and fluid interfaces. Clearly, continuum-scale processes and colloid- and surface-scale processes act in tandem in a drying drop. Thus, drying drops and the patterns they leave behind represent an attractive area of study from the perspective of both fundamental science and applications.

Due to the variety and nature of the processes involved at various scales, current research seems to be taking two different directions. The first involves drying drops of complex fluids, which primarily modify the microscopic interactions between the dispersed entities and the surrounding environment, thereby altering the colloidal science in the system. The second involves drying drops in complex configurations, where macroscopic transport phenomena, mainly the evaporation process, are altered. Even in situ measurements and characterization of temperature and velocity profiles in the case of a simple sessile drop are challenging. Research in both directions is ongoing, and significant progress in certain aspects has been made. However, our understanding remains incomplete, as discussed in Sections 6 and 7. Needless to say, the combination of these two cases is much less well investigated. While this review has been devoted essentially to analyzing the evaporation of and resulting patterns from a single drop, mass transfer–mediated interaction between multiple drops is a promising field of research (128–131).

The lack of a complete understanding of the relevant processes in a drying drop is also reflected in the literature as the absence of a predictive theory or a universal simulation model that can be used in a variety of situations. While this lack is understandable, considering the complexity and the range of scales involved in the problem, further efforts are required to unify the existing framework of models.

The two major potential applications of studying drying drops of colloidal dispersions are (*a*) achieving self-assembly of nanoparticles and colloidal particles on unprecedentedly long length scales and (*b*) suppressing inhomogeneous distributions of particles in dried patterns, desirable in printing and coating applications. Significant investigations have been devoted to both applications; however, a reliable and universal solution has yet to emerge and be practiced. Still another projected application is the development of low-cost medical devices for disease diagnosis. Significant progress has yet to be made in this direction as well.

DISCLOSURE STATEMENT

The authors are not aware of any affiliations, memberships, funding, or financial holdings that might be perceived as affecting the objectivity of this review.

ACKNOWLEDGMENTS

We acknowledge financial support from the Science and Engineering Research Board, Department of Science and Technology, Government of India (grant CRG/2020/003643). We are grateful for financial support from the Indian Institute of Technology Madras through the Institutions of Eminence Scheme, Ministry of Education (formerly the Ministry of Human Resource Development), Government of India.

LITERATURE CITED

1. Larson RG. 2012. Re-shaping the coffee ring. *Angew. Chem. Int. Ed.* 51:2546–48
2. De Gennes PG, Brochard-Wyart F, Quéré D. 2013. *Capillarity and Wetting Phenomena: Drops, Bubbles, Pearls, Waves*. New York: Springer
3. Sefiane K. 2014. Patterns from drying drops. *Adv. Colloid Interface Sci.* 206:372–81

4. Larson RG. 2014. Transport and deposition patterns in drying sessile droplets. *AIChE J.* 60:1538–71
5. Kovalchuk N, Trybala A, Starov V. 2014. Evaporation of sessile droplets. *Curr. Opin. Colloid Interface Sci.* 19:336–42
6. Larson RG. 2017. Twenty years of drying droplets. *Nature* 550:466–67
7. Giorgiutti-Dauphiné F, Pauchard L. 2018. Drying drops. *Eur. Phys. J. E* 41:32
8. Mampallil D, Eral HB. 2018. A review on suppression and utilization of the coffee-ring effect. *Adv. Colloid Interface Sci.* 252:38–54
9. Zang D, Tarafdar S, Tarasevich YY, Choudhury MD, Dutta T. 2019. Evaporation of a droplet: from physics to applications. *Phys. Rep.* 804:1–56
10. Cossali GE, Tonini S. 2021. *Drop Heating and Evaporation: Analytical Solutions in Curvilinear Coordinate Systems*. Berlin: Springer
11. Lohse D. 2022. Fundamental fluid dynamics challenges in inkjet printing. *Annu. Rev. Fluid Mech.* 54:349–82
12. Gelderblom H, Diddens C, Marin A. 2022. Evaporation-driven liquid flow in sessile droplets. *Soft Matter* 18:8535–53
13. Wilson SK, D'Ambrosio HM. 2023. Evaporation of sessile droplets. *Annu. Rev. Fluid Mech.* 55:481–509
14. Brown R. 1829. Additional remarks on active molecules. *Philos. Mag.* 6:161–66
15. Kulnis WJ Jr., Unertl WN. 1994. A thermal stage for nanoscale structure studies with the scanning force microscope. In *Determining Nanoscale Physical Properties of Materials by Microscopy and Spectroscopy*, ed. M Sarikaya, HK Wickramasinghe, M Isaacson, pp. 105–8. Pittsburgh, PA: Mater. Res. Soc.
16. El Bediwi A, Kulnis W, Luo Y, Woodland D, Unertl W. 1994. Distributions of latex particles deposited from water suspensions. *MRS Online Proc. Libr.* 372:277–82
17. Vanderhoff J, Gurnee E. 1956. A motion picture investigation of polymer latex phenomena. *Tappi J.* 39:71–77
18. Deegan RD, Bakajin O, Dupont TF, Huber G, Nagel SR, Witten TA. 1997. Capillary flow as the cause of ring stains from dried liquid drops. *Nature* 389:827–29
19. Deegan RD, Bakajin O, Dupont TF, Huber G, Nagel SR, Witten TA. 2000. Contact line deposits in an evaporating drop. *Phys. Rev. E* 62:756–65
20. Han W, Lin Z. 2012. Learning from "coffee rings": ordered structures enabled by controlled evaporative self-assembly. *Angew. Chem. Int. Ed.* 51:1534–46
21. Anyfantakis M, Baigl D. 2015. Manipulating the coffee-ring effect: interactions at work. *ChemPhysChem* 16:2726–34
22. Parsa M, Harmand S, Sefiane K. 2018. Mechanisms of pattern formation from dried sessile drops. *Adv. Colloid Interface Sci.* 254:22–47
23. Dugyala VR, Daware SV, Basavaraj MG. 2013. Shape anisotropic colloids: synthesis, packing behavior, evaporation driven assembly, and their application in emulsion stabilization. *Soft Matter* 9:6711–25
24. Shao X, Duan F, Hou Y, Zhong X. 2019. Role of surfactant in controlling the deposition pattern of a particle-laden droplet: fundamentals and strategies. *Adv. Colloid Interface Sci.* 275:102049
25. Bhardwaj R, Fang X, Somasundaran P, Attinger D. 2010. Self-assembly of colloidal particles from evaporating droplets: role of DLVO interactions and proposition of a phase diagram. *Langmuir* 26:7833–42
26. Kuncicky DM, Velev OD. 2008. Surface-guided templating of particle assemblies inside drying sessile droplets. *Langmuir* 24:1371–80
27. Bansal L, Seth P, Murugappan B, Basu S. 2018. Suppression of coffee ring: (Particle) size matters. *Appl. Phys. Lett.* 112:211605
28. Mondal R, Semwal S, Kumar PL, Thampi SP, Basavaraj MG. 2018. Patterns in drying drops dictated by curvature-driven particle transport. *Langmuir* 34:11473–83
29. Yang X, Li CY, Sun Y. 2014. From multi-ring to spider web and radial spoke: competition between the receding contact line and particle deposition in a drying colloidal drop. *Soft Matter* 10:4458–63
30. Parthasarathy D, Thampi SP, Ravindran P, Basavaraj MG. 2021. Further insights into patterns from drying particle laden sessile drops. *Langmuir* 37:4395–402
31. Dugyala VR, Basavaraj MG. 2014. Control over coffee-ring formation in evaporating liquid drops containing ellipsoids. *Langmuir* 30:8680–86

32. Mayarani M, Basavaraj MG, Satapathy DK. 2017. Loosely packed monolayer coffee stains in dried drops of soft colloids. *Nanoscale* 9:18798–803
33. Marín ÁG, Gelderblom H, Lohse D, Snoeijer JH. 2011. Order-to-disorder transition in ring-shaped colloidal stains. *Phys. Rev. Lett.* 107:085502
34. Dugyala VR, Basavaraj MG. 2015. Evaporation of sessile drops containing colloidal rods: coffee-ring and order–disorder transition. *J. Phys. Chem. B* 119:3860–67
35. Hu H, Larson RG. 2006. Marangoni effect reverses coffee-ring depositions. *J. Phys. Chem. B* 110:7090–94
36. Yunker PJ, Still T, Lohr MA, Yodh A. 2011. Suppression of the coffee-ring effect by shape-dependent capillary interactions. *Nature* 476:308–11
37. Still T, Yunker PJ, Yodh AG. 2012. Surfactant-induced Marangoni eddies alter the coffee rings of evaporating colloidal drops. *Langmuir* 28:4984–88
38. Cui L, Zhang J, Zhang X, Huang L, Wang Z, et al. 2012. Suppression of the coffee ring effect by hydrosoluble polymer additives. *ACS Appl. Mater. Interfaces* 4:2775–80
39. Rey M, Walter J, Harrer J, Perez CM, Chiera S, et al. 2022. Versatile strategy for homogeneous drying patterns of dispersed particles. *Nat. Commun.* 13:2840
40. Parsa M, Harmand S, Sefiane K, Bigerelle M, Deltombe R. 2015. Effect of substrate temperature on pattern formation of nanoparticles from volatile drops. *Langmuir* 31:3354–67
41. Lama H, Satapathy DK, Basavaraj MG. 2020. Modulation of central depletion zone in evaporated sessile drops via substrate heating. *Langmuir* 36:4737–44
42. Li Y, Yang Q, Li M, Song Y. 2016. Rate-dependent interface capture beyond the coffee-ring effect. *Sci. Rep.* 6:24628
43. Morinaga K, Oikawa N, Kurita R. 2018. Emergence of different crystal morphologies using the coffee ring effect. *Sci. Rep.* 8:12503
44. Shimobayashi SF, Tsudome M, Kurimura T. 2018. Suppression of the coffee-ring effect by sugar-assisted depinning of contact line. *Sci. Rep.* 8:17769
45. Ding Y, Ling J, Qiao Y, Li Z, Sun Z, et al. 2016. A high-throughput fluorimetric microarray with enhanced fluorescence and suppressed "coffee-ring" effects for the detection of calcium ions in blood. *Sci. Rep.* 6:38602
46. Mayarani M, Basavaraj MG, Satapathy DK. 2018. Viscoelastic particle–laden interface inhibits coffee-ring formation. *Langmuir* 34:14294–301
47. Sempels W, De Dier R, Mizuno H, Hofkens J, Vermant J. 2013. Auto-production of biosurfactants reverses the coffee ring effect in a bacterial system. *Nat. Commun.* 4:1757
48. Anyfantakis M, Geng Z, Morel M, Rudiuk S, Baigl D. 2015. Modulation of the coffee-ring effect in particle/surfactant mixtures: the importance of particle–interface interactions. *Langmuir* 31:4113–20
49. Li Y, Lv C, Li Z, Quéré D, Zheng Q. 2015. From coffee rings to coffee eyes. *Soft Matter* 11:4669–73
50. Lama H, Basavaraj MG, Satapathy DK. 2017. Tailoring crack morphology in coffee-ring deposits via substrate heating. *Soft Matter* 13:5445–52
51. Mampallil D, Reboud J, Wilson R, Wylie D, Klug DR, Cooper JM. 2015. Acoustic suppression of the coffee-ring effect. *Soft Matter* 11:7207–13
52. Man X, Doi M. 2016. Ring to mountain transition in deposition pattern of drying droplets. *Phys. Rev. Lett.* 116:066101
53. Du X, Deegan R. 2015. Ring formation on an inclined surface. *J. Fluid Mech.* 775:R3
54. Gopu M, Rathod S, Namangalam U, Pujala RK, Kumar SS, Mampallil D. 2020. Evaporation of inclined drops: formation of asymmetric ring patterns. *Langmuir* 36:8137–43
55. Kumar PL, Thampi SP, Basavaraj MG. 2021. Patterns from drops drying on inclined substrates. *Soft Matter* 17:7670–81
56. Shmuylovich L, Shen AQ, Stone HA. 2002. Surface morphology of drying latex films: multiple ring formation. *Langmuir* 18:3441–45
57. Mondal R, Basavaraj MG. 2019. Influence of the drying configuration on the patterning of ellipsoids—concentric rings and concentric cracks. *Phys. Chem. Chem. Phys.* 21:20045–54
58. Srivastava S, Wahith ZA, Gang O, Colosqui CE, Bhatia SR. 2020. Dual-scale nanostructures via evaporative assembly. *Adv. Mater. Interfaces* 7:1901954

59. Maheshwari S, Zhang L, Zhu Y, Chang HC. 2008. Coupling between precipitation and contact-line dynamics: multiring stains and stick-slip motion. *Phys. Rev. Lett.* 100:044503
60. Frastia L, Archer AJ, Thiele U. 2011. Dynamical model for the formation of patterned deposits at receding contact lines. *Phys. Rev. Lett.* 106:077801
61. Mondal R, Basavaraj MG. 2020. Patterning of colloids into spirals via confined drying. *Soft Matter* 16:3753–61
62. Thampi SP, Basavaraj MG. 2020. Beyond coffee rings: drying drops of colloidal dispersions on inclined substrates. *ACS Omega* 5:11262–70
63. Langmuir I. 1918. The evaporation of small spheres. *Phys. Rev.* 12:368–70
64. Popov YO. 2005. Evaporative deposition patterns: spatial dimensions of the deposit. *Phys. Rev. E* 71:036313
65. Hu H, Larson RG. 2002. Evaporation of a sessile droplet on a substrate. *J. Phys. Chem. B* 106:1334–44
66. Sáenz P, Wray A, Che Z, Matar O, Valluri P, et al. 2017. Dynamics and universal scaling law in geometrically-controlled sessile drop evaporation. *Nat. Commun.* 8:14783
67. Ristenpart W, Kim P, Domingues C, Wan J, Stone HA. 2007. Influence of substrate conductivity on circulation reversal in evaporating drops. *Phys. Rev. Lett.* 99:234502
68. Kaplan CN, Mahadevan L. 2015. Evaporation-driven ring and film deposition from colloidal droplets. *J. Fluid Mech.* 781:R2
69. Ryu S, Kim JY, Kim SY, Weon BM. 2017. Drying-mediated patterns in colloid-polymer suspensions. *Sci. Rep.* 7:1079
70. Hu H, Larson RG. 2005. Analysis of the microfluid flow in an evaporating sessile droplet. *Langmuir* 21:3963–71
71. Hu H, Larson RG. 2005. Analysis of the effects of Marangoni stresses on the microflow in an evaporating sessile droplet. *Langmuir* 21:3972–80
72. Nguyen VX, Stebe KJ. 2002. Patterning of small particles by a surfactant-enhanced Marangoni-Bénard instability. *Phys. Rev. Lett.* 88:164501
73. Marin A, Liepelt R, Rossi M, Kähler CJ. 2016. Surfactant-driven flow transitions in evaporating droplets. *Soft Matter* 12:1593–600
74. Edwards A, Atkinson P, Cheung C, Liang H, Fairhurst D, Ouali F. 2018. Density-driven flows in evaporating binary liquid droplets. *Phys. Rev. Lett.* 121:184501
75. Li Y, Diddens C, Lv P, Wijshoff H, Versluis M, Lohse D. 2019. Gravitational effect in evaporating binary microdroplets. *Phys. Rev. Lett.* 122:114501
76. Davidson ZS, Huang Y, Gross A, Martinez A, Still T, et al. 2017. Deposition and drying dynamics of liquid crystal droplets. *Nat. Commun.* 8:15642
77. Xu T, Lam ML, Chen TH. 2017. Discrete element model for suppression of coffee-ring effect. *Sci. Rep.* 7:42817
78. Crivoi A, Duan F. 2014. Three-dimensional Monte Carlo model of the coffee-ring effect in evaporating colloidal droplets. *Sci. Rep.* 4:4310
79. Yu YS, Wang MC, Huang X. 2017. Evaporative deposition of polystyrene microparticles on PDMS surface. *Sci. Rep.* 7:14118
80. Semenov S, Trybala A, Agogo H, Kovalchuk N, Ortega F, et al. 2013. Evaporation of droplets of surfactant solutions. *Langmuir* 29:10028–36
81. Wu M, Di Y, Man X, Doi M. 2019. Drying droplets with soluble surfactants. *Langmuir* 35:14734–41
82. Seo C, Jang D, Chae J, Shin S. 2017. Altering the coffee-ring effect by adding a surfactant-like viscous polymer solution. *Sci. Rep.* 7:500
83. Mayarani M, Basavaraj MG, Satapathy DK. 2021. Colloidal monolayers with cell-like tessellations via interface assisted evaporative assembly. *J. Colloid Interface Sci.* 583:683–91
84. Basu N, Mukherjee R. 2020. Evaporative drying of sodium chloride solution droplet on a thermally controlled substrate. *J. Phys. Chem. B* 124:1266–74
85. Dewangan JK, Basu N, Chowdhury M. 2022. Cationic surfactant-directed structural control of NaCl crystals from evaporating sessile droplets. *Soft Matter* 18:62–79
86. Shahidzadeh N, Schut MF, Desarnaud J, Prat M, Bonn D. 2015. Salt stains from evaporating droplets. *Sci. Rep.* 5:10335

87. McBride SA, Dash S, Khan S, Varanasi KK. 2019. Evaporative crystallization of spirals. *Langmuir* 35:10484–90
88. Hu G, Yang L, Yang Z, Wang Y, Jin X, et al. 2020. A general ink formulation of 2D crystals for wafer-scale inkjet printing. *Sci. Adv.* 6:eaba5029
89. Pahlavan AA, Yang L, Bain CD, Stone HA. 2021. Evaporation of binary-mixture liquid droplets: the formation of picoliter pancakelike shapes. *Phys. Rev. Lett.* 127:024501
90. Bittermann M, Deblais A, Lépinay S, Bonn D, Shahidzadeh N. 2020. Deposits from evaporating emulsion drops. *Sci. Rep.* 10:14863
91. Gopu M, Mampallil D. 2022. Distributed evaporation of water-in-oil emulsion drops on solid surfaces. *Phys. Fluids* 34:102110
92. Guo W, Kinghorn AB, Zhang Y, Li Q, Poonam AD, et al. 2021. Non-associative phase separation in an evaporating droplet as a model for prebiotic compartmentalization. *Nat. Commun.* 12:3194
93. Weber CA, Zwicker D, Jülicher F, Lee CF. 2019. Physics of active emulsions. *Rep. Prog. Phys.* 82:064601
94. Xu L, Berges A, Lu PJ, Studart AR, Schofield AB, et al. 2010. Drying of complex suspensions. *Phys. Rev. Lett.* 104:128303
95. Smalyukh II, Zribi OV, Butler JC, Lavrentovich OD, Wong GC. 2006. Structure and dynamics of liquid crystalline pattern formation in drying droplets of DNA. *Phys. Rev. Lett.* 96:177801
96. Nerger BA, Brun PT, Nelson CM. 2020. Marangoni flows drive the alignment of fibrillar cell–laden hydrogels. *Sci. Adv.* 6:eaaz7748
97. Yunker PJ, Gratale M, Lohr MA, Still T, Lubensky TC, Yodh AG. 2012. Influence of particle shape on bending rigidity of colloidal monolayer membranes and particle deposition during droplet evaporation in confined geometries. *Phys. Rev. Lett.* 108:228303
98. Kim DO, Pack M, Hu H, Kim H, Sun Y. 2016. Deposition of colloidal drops containing ellipsoidal particles: competition between capillary and hydrodynamic forces. *Langmuir* 32:11899–906
99. Sefiane K. 2010. On the formation of regular patterns from drying droplets and their potential use for bio-medical applications. *J. Bionic Eng.* 7:S82–93
100. Yakhno T, Yakhno V. 2009. Structural evolution of drying drops of biological fluids. *Tech. Phys.* 54:1219–27
101. Sobac B, Brutin D. 2011. Structural and evaporative evolutions in desiccating sessile drops of blood. *Phys. Rev. E* 84:011603
102. Brutin D, Sobac B, Loquet B, Sampol J. 2011. Pattern formation in drying drops of blood. *J. Fluid Mech.* 667:85–95
103. Esmonde-White KA, Mandair GS, Raaii F, Jacobson JA, Miller BS, et al. 2009. Raman spectroscopy of synovial fluid as a tool for diagnosing osteoarthritis. *J. Biomed. Opt.* 14:034013
104. Esmonde-White KA, Mandair GS, Esmonde-White FW, Raaii F, Roessler BJ, Morris MD. 2009. Osteoarthritis screening using Raman spectroscopy of dried human synovial fluid drops. *Proc. SPIE* 7166:152–59
105. McLane J, Wu C, Khine M. 2015. Enhanced detection of protein in urine by droplet evaporation on a superhydrophobic plastic. *Adv. Mater. Interfaces* 2:1400034
106. Esmonde-White KA, Esmonde-White FW, Morris MD, Roessler BJ. 2014. Characterization of biofluids prepared by sessile drop formation. *Analyst* 139:2734–41
107. Andac T, Weigmann P, Velu SK, Pinçe E, Volpe G, et al. 2019. Active matter alters the growth dynamics of coffee rings. *Soft Matter* 15:1488–96
108. Kasyap T, Koch DL, Wu M. 2014. Bacterial collective motion near the contact line of an evaporating sessile drop. *Phys. Fluids* 26:111703
109. Ma X, Liu Z, Zeng W, Lin T, Tian X, Cheng X. 2022. Crack patterns of drying dense bacterial suspensions. *Soft Matter* 18:5239–48
110. Parneix C, Vandoolaeghe P, Nikolayev V, Quéré D, Li J, Cabane B. 2010. Dips and rims in dried colloidal films. *Phys. Rev. Lett.* 105:266103
111. Harris DJ, Hu H, Conrad JC, Lewis JA. 2007. Patterning colloidal films via evaporative lithography. *Phys. Rev. Lett.* 98:148301
112. Xu J, Xia J, Hong SW, Lin Z, Qiu F, Yang Y. 2006. Self-assembly of gradient concentric rings via solvent evaporation from a capillary bridge. *Phys. Rev. Lett.* 96:066104

113. Chattopadhyay A, Hegde O, Basu S, et al. 2022. Malleable patterns from the evaporation of colloidal liquid bridge: coffee ring to the scallop shell. arXiv:2201.02382 [cond-mat.soft]
114. Lin Z, Granick S. 2005. Patterns formed by droplet evaporation from a restricted geometry. *J. Am. Chem. Soc.* 127:2816–17
115. Wells GG, Ruiz-Gutiérrez É, Le Lirzin Y, Nourry A, Orme BV, et al. 2018. Snap evaporation of droplets on smooth topographies. *Nat. Commun.* 9:1380
116. Kim S, Kim WY, Nam SH, Shin S, Choi SH, et al. 2021. Microstructured surfaces for reducing chances of fomite transmission via virus-containing respiratory droplets. *ACS Nano* 15:14049–60
117. Vakarelski IU, Chan DY, Nonoguchi T, Shinto H, Higashitani K. 2009. Assembly of gold nanoparticles into microwire networks induced by drying liquid bridges. *Phys. Rev. Lett.* 102:058303
118. Yen TM, Fu X, Wei T, Nayak RU, Shi Y, Lo YH. 2018. Reversing coffee-ring effect by laser-induced differential evaporation. *Sci. Rep.* 8:3157
119. Bahns J, Sankaranarayanan S, Gray S, Chen L. 2011. Optically directed assembly of continuous mesoscale filaments. *Phys. Rev. Lett.* 106:095501
120. Farzeena C, Varanakkottu SN. 2022. Patterning of metallic nanoparticles over solid surfaces from sessile droplets by thermoplasmonically controlled liquid flow. *Langmuir* 38:2003–13
121. Kim JY, Hwang IG, Weon BM. 2017. Evaporation of inclined water droplets. *Sci. Rep.* 7:42848
122. Extrand CW, Kumagai Y. 1995. Liquid drops on an inclined plane: the relation between contact angles, drop shape, and retentive force. *J. Colloid Interface Sci.* 170:515–21
123. Quéré D, Azzopardi MJ, Delattre L. 1998. Drops at rest on a tilted plane. *Langmuir* 14:2213–16
124. Bansal L, Seth P, Sahoo S, Mukherjee R, Basu S. 2018. Beyond coffee ring: anomalous self-assembly in evaporating nanofluid droplet on a sticky biomimetic substrate. *Appl. Phys. Lett.* 113:213701
125. Timm M, Dehdashti E, Jarrahi Darban A, Masoud H. 2019. Evaporation of a sessile droplet on a slope. *Sci. Rep.* 9:19803
126. Charitatos V, Pham T, Kumar S. 2021. Droplet evaporation on inclined substrates. *Phys. Rev. Fluids* 6:084001
127. Dhar P, Dwivedi RK, Harikrishnan A. 2020. Surface declination governed asymmetric sessile droplet evaporation. *Phys. Fluids* 32:112010
128. Cira NJ, Benusiglio A, Prakash M. 2015. Vapour-mediated sensing and motility in two-component droplets. *Nature* 519:446–50
129. Pandey K, Hatte S, Pandey K, Chakraborty S, Basu S. 2020. Cooperative evaporation in two-dimensional droplet arrays. *Phys. Rev. E* 101:043101
130. Wray AW, Duffy BR, Wilson SK. 2020. Competitive evaporation of multiple sessile droplets. *J. Fluid Mech.* 884:A45
131. Masoud H, Howell PD, Stone HA. 2021. Evaporation of multiple droplets. *J. Fluid Mech.* 927:R4